POLITECNICO DI TORINO
DEPARTMENT OF MECHANICAL AND AEROSPACE ENGINEERING
MASTER'S DEGREE IN MECHANICAL ENGINEERING

MECHANICAL DESIGN AND CONTROL OF DEPLOYABLE POINTING MECHANISM DEVELOPED FOR LUNAR MICROSATELLITE APPLICATIONS

Master Thesis of:
Thomas JANSEN

Academic Supervisor:
Prof. Aurelio SOMA'

Company Supervisor:
Ing. Silvio PATRUNO

argotec
our boost to your future

Abstract

The aim of this Thesis consists in the design of a pointing mechanism for a High gain antenna, used for a lunar-terrestrial telecommunication satellite constellation.
The pointing structure is based on the Canfield joint mechanism, since the antenna needs to point in any direction over a hemisphere, and at the same time present a compact stowed configuration. This system will allow small satellites, like microsatellites, to have additional Degree of freedom (Dof) to handle complex missions previously manageable just by big satellites.
The main focus is to design a platform manipulator compact, cheap to produce, reliably able to guarantee the pointing characteristics, and easily mass-produced for constellation purposes.
The design was guided through a parametric MATLAB code to allow the kinematic and dynamical analysis to bring changes to the geometry of the structure obtaining the optimized dimensions for the specific application.
A bio-inspired design is obtained, able to guarantee mechanical protection in case of a controller failure and with great workspace robustness and maneuverability.

To my family, for all their support
and to all the inspiring people I met in these years
who allowed me to grow professionally and personally.

Contents

List of Figures

List of Tables

Chapter 1

Introduction

1-1 Argotec

Figure 1-1: Argotec Logo [1]

As part of the thesis in the company of the Polytechnic of Turin, the following thesis was developed at the company Argotec srl, an Italian aerospace engineering company whose activities mainly concern the production of microsatellites for deep space (Fig.1-2a) and the development of innovative solutions in order to improve and to support the life and the comfort of space explorers (Fig.1-2b). The company activities follow the “all in-house concept” including design, development, integration, qualification and operation services.

In the company the need has emerged to develop the mechanical design of a deployable pointing mechanism that can be used on microsatellites.

Since the small satellite segment is in fast development, in particular for deep space missions, the need for more complex small satellite is needed to allow more complex missions to be executed.
Current CubeSat are design to be as simple and as cheep as possible, but this simplicity can also be a drawback since a simple design causes the system to be limited in the tasks that its able to do. For these reason the need for a still small and cheep structure, but with the capability of executing tasks that were previously possible only on big satellites is growing.

(a) 6U Cubesat integration


(b) Argotec Mission Control Center

One of the main differences between a current large satellite and a CubeSat lies in the limited number of degrees of freedom that the CubeSat has. This limitation sometimes conditions the satellite to execute one task at the time or even make the satellite incompatible with the needed mission. To respond to this need a mechanical robotic structure able to guarantee this additional structure adaptability was developed. This type of robotic structure can be used in a variety of applications such as the maneuvering of a thruster, which allows for both orbital adjustment and thrust-driven attitude control, or the precise pointing of an antenna. This is the exact need of Argotec's new lunar project Andromeda [1].

Andromeda is a satellite constellation orbiting around the Moon to allow the hardware and future astronauts to be able to communicate reliably with Earth. To respond to this need there must be an additional degree of freedom in the satellite that allows the independent control of the antenna that must point to the surface with respect to the antenna that needs to be pointed to Earth. The solution to this problem was found with the the pointing mechanism that was developed in this thesis.

1-1-1 Motivation and Problem Definition

To be able to guarantee a reliable wireless connection, a High gain antenna will be mounted on every CubeSat of the constellation that will be pointed towards the earth. To allow this task a pointing mechanism with high dexterity, allowing the antenna to be pointed in any direction over a hemisphere, should be designed.

One of the main requirements for the pointing mechanism is its total envelope in the stowed configuration since the structure has to be as compact and light as possible.

Since the pointing mechanism is intended for use on a constellation of satellites, the design should be preferably modular, easy to manufacture, and with extended use of standard hardware to reduce the price.

This pointing system will be used with a traditional RF communication system, but its precision will be particularly critical for possible future advanced optical communication. In fact the primary benefit of optical communications for space missions, especially mid and deep space missions, is to dramatically increase the amount of data that can be sent back to

Earth [7], but at the same time the main drawback of an optical system is that the pointing mechanism needs to be extremely accurate to allow the correct pointing of the optical signal to the ground station.

For all previous examined reasons the pointing mechanism should be:

- Light and small
- Able to point over an hemisphere
- With high pointing resolution
- Reliable
- Able to withstand the space environmental condition for five years

Chapter 2

Recalls of robotics

The robot is the combination of various mechanical and electrical components that allows the machine to perform the required task. The main components are:

- The manipulator:
  the mechanical part of the robot which consists of a set of rigid bodies (links) connected by joints
- The actuators:
  which impose movement on the manipulator through the actuation of the joints
- The sensors:
  which measure the state of the manipulator
- The control unit:
  witch controls the manipulator movements

2-1 Key concepts

- **Degree of freedom (Dof)**
  Each joint introduces some relative degree of movement between the two links connected by the joint. On the other hand, the Dof are the possible degree of motion of the final End-effector. To develop a 6 Dof robot (3 positions and 3 orientation in the 3D space) at least 6 degrees of movement in total are necessary. A robot is defined *Redundant* if the total number of degree of motion is higher than the Dof of the system.

- **Singularity configurations:**
  These are particular position configurations in which the end effector loses instantaneously some Dof. This causes the robot to lose control and the kinematic and dynamic constraints show singularity.

- **Robot workspace:**
  3D domain in which the end effector can move. It depends on the robot dimensions and the kinematic structure. It can be distinguished into two types:
  - Primary type (or reachable): set of points reachable by the end effector.
  - Secondary type (or dexterity type): set of points reachable with the desired orientation.
    This is the main workspace that we will consider in this paper since in our pointing mechanism the orientation of the end effector is the main objective.
    This workspace type has a smaller 3D domain but there are multi-model approaches that allow parallel robots to cross Type 2 singularities. The main idea is to shift near singularities to a simplified dynamic model that can never degenerate [8].
- **Pointing precision:**
  - Position repeatability:
    ability of the end effector to return to a certain position.
  - Accuracy:
    precision with which the end effector is able to reach the theoretical position required (distance between the desired position and the actual position).

  Systematic errors cause accuracy problems, while the random errors cause repeatability problems. Possible errors causes are:
  - Structural errors
  - Mechanical play between the parts
  - Sensor and actuators resolution
- **Reference frames:**
  - Joint Coordinates:
    Scalar quantities that determine the relative disposition of the links of the kinematic pair are referred to as manipulator joint coordinates. In revolute joints, the joint coordinate is the rotation angle, while in prismatic joints the joint coordinate represents the displacement along the joint axis.
  - External coordinates:
    External (operational, world) coordinates describe manipulator end-effector position and orientation with respect to some reference coordinate system. The reference system is chosen to suit a particular application. Most frequently, a fixed coordinate frame attached to the manipulator base is considered as the reference system. The manipulator hand position is usually described by Cartesian coordinates x, y, and z (Fig.2-1)[2]. In this application, the pointing requires the control not only of the manipulator's hand position but also of hand orientation with the objects located in the manipulator workspace. The orientation is usually specified

by Euler angles between the coordinate frame attached to the last (n-th) link and the reference system (Fig.2-1). We will consider the yaw angle ψ, the pitch angle θ, and the roll angle ϕ. The yaw angle corresponds to a rotation ψ about the z-axis, pitch corresponds to a rotation θ about the new y-axis, and roll corresponds to a rotation ϕ about the new x-axis [2].

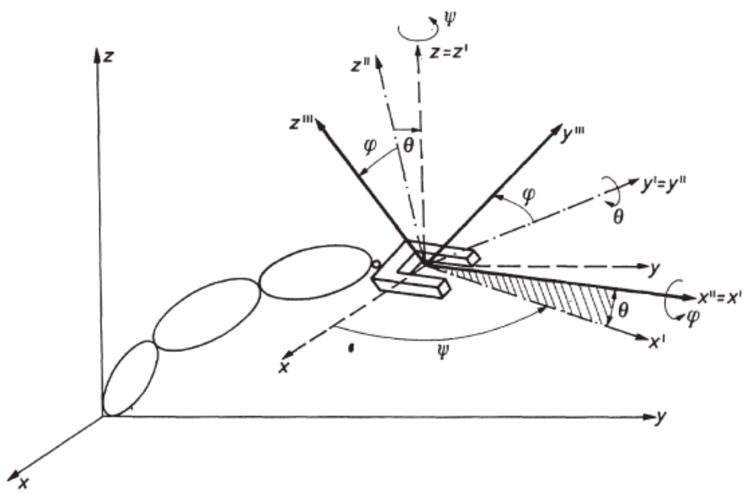

Figure 2-1: Manipulator external coordinates[2]

Chapter 3

Review of the state of the art

3-1 Pointing

There are various pointing solutions use in the space sector for tasks such as thruster maneuvering, target tracking for communication between air to ground/air to air systems, and camera pointing purposes.
In the majority of these cases, the conventional 2-axis gimbals are preferred since they are easy to control with high precision and they are simple in design [9]. In particular cases, more complex solutions are preferred to eliminate some drawbacks of the standard 2 axis gimbal configuration.
A mechanism can be identified depending on the arrangement of its connections and joints. The three main classes are:

- Serial mechanism
- Parallel mechanism
- Hybrid mechanism

Serial mechanisms are the ones that present a sequential connection of the various parts of the system through joints and links. The joints can be of different nature, but in the majority of cases, the structure is composed of two revolute joints.
The parallel Mechanism is designed as a parallel connection of 2 or more serial chains mechanism that connects the base of the system to a common point called the endpoint. This type of mechanism has a more rigid structure than the serial ones, which allows them to have smaller pointing errors, but as a downside, the kinematic/dynamics and control of the system are more complicated.
The hybrid mechanism is a chain of one or more parallel and serial mechanism.

In this thesis after a trade-off between a serial and parallel design, the parallel configuration is preferred since a high pointing precision is needed and it was demonstrated that such kinematics allows the system to maintain a wide workspace in the possibility of a failure, when one degree of freedom is lost.

3-2 Parallel Mechanisms Concepts

There are different parallel mechanism configurations present in the literature. We will investigate all the most common design before developing one for the specific case

3-2-1 Omini-Wrist Family

Multiple mechanisms are designed and patented by the company Rose-Hime Designs. Parallel mechanisms manufactured by the company created under the family name of "Omni-Wrist". Omni-Wrist III, Omni-Wrist V, and Omni-Wrist VI are described on the company website [3].

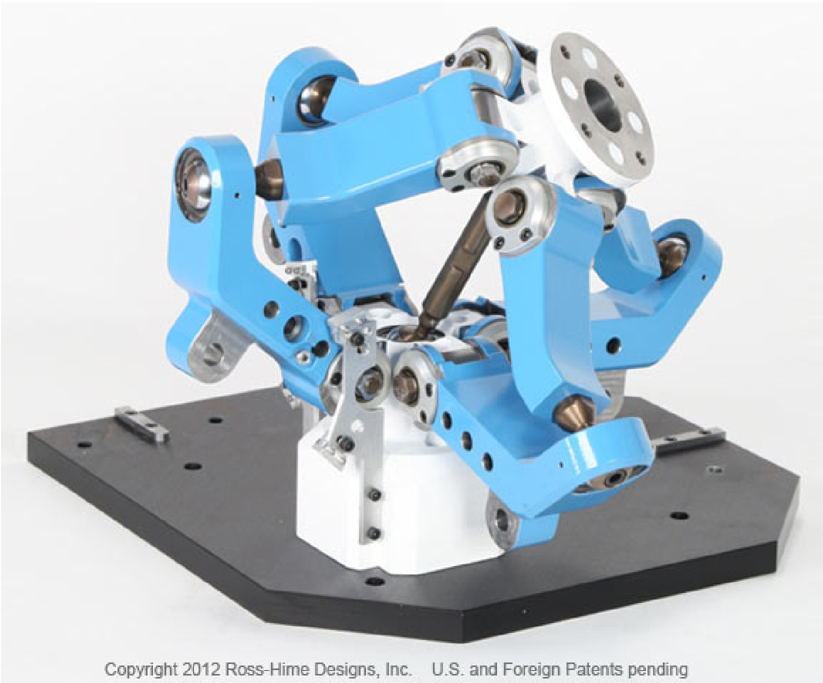

Figure 3-1: Omni-Wrist VI [3]

3-2-2 Wide Angle Gimbal

Wide Angle Gimbal is a 4R4 mechanism used for optical applications by Sofka [4],and Nikulin [10]. The mechanism is in the form of a parallel robotic linkage that consists of four arms, each comprised of three links and four joints that connect the stationary base to the device platform as in Fig.3-2. Two rotary actuators drive two of the four links attached to the stationary platform to achieve a full hemisphere motion.

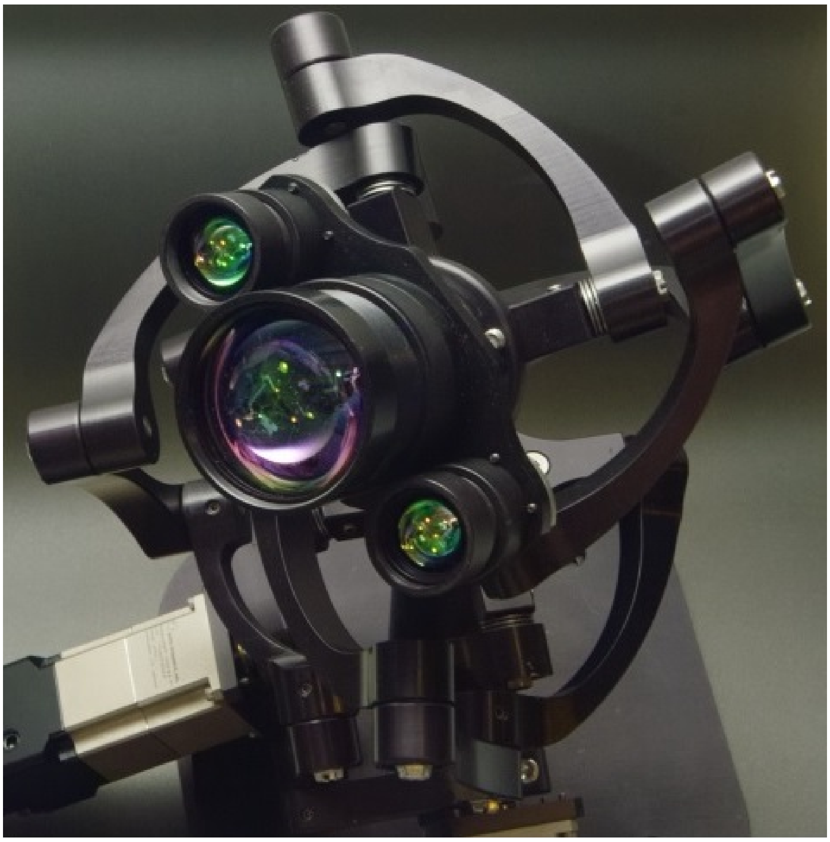

Figure 3-2: Wide Angle Gimbal [4]

3-2-3 Monolithic Mechanism

Merriam in the paper [5] uses a monolithic structure as a pointing device for application in spacecraft thruster, antenna, or solar array systems which can be seen in Fig.3-3 . This 3D-printed structure is made of titanium. As a result of being a monolithic structure, the system moves only with bending motion. Manipulator contains no bearings and actuators bend/elastically deform the material. This structure is proposed as a candidate for space applications. In a zero pressure environment, it is challenging to use bearings since lubrication tends to disperse. The bearingless design eliminates many frictions, backlash, lubrication, and wear problems that occur in low environmental pressure.

Figure 3-3: Monolithic 2 Degree of freedom (Dof) fully compliant space pointing mechanism [5]

3-2-4 Canfield Joint

The Carpal Wrist, also called Canfield Joint from the name of his inventor Dr. Stephen Canfield of the Tennessee Tech University, was designed by taking inspiration from the Human wrist [6]. It presents eight primary links, corresponding to the eight carpi bones, that enclose a protected tunnel that can be used for routing of electrical cables, much like the carpal tunnel, and a parallel actuation scheme, similar to the flexor and extensor carpi muscles along the forearm.

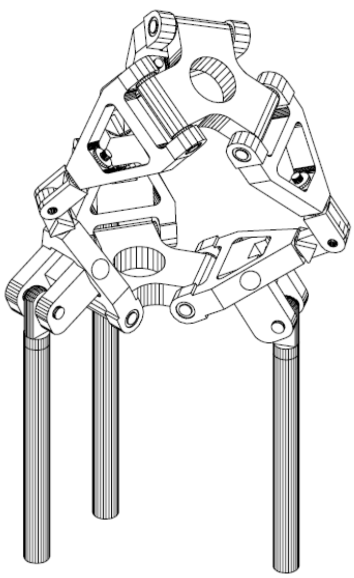

Figure 3-4: Canfield joint CAD model [6]

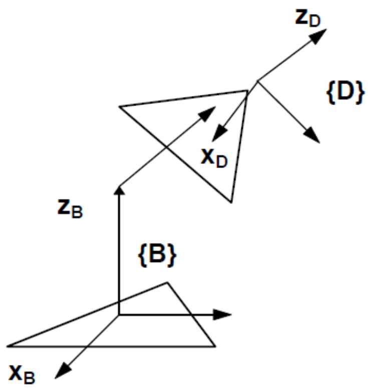

Figure 3-5: End-effector reference frame [6]

Like other parallel manipulator models, it shows high rigidity and large payload to weight capabilities, but few are been developed for application because of the complicated kinematics and dynamics modeling. The mathematical model of the system is necessary for the motion control of any kind of manipulator. Indeed the model can output the required motor movement needed to follow the desired robot motion reserved as input.

The Canfield Joint has three Dof and can be controlled using three actuators attached to the base in strategic positions. The control of the three angles through the command of the motors positioned at the base allows for full hemispherical motion.

The three Dof controlled are the pitch angle θ (rotation along the y axis), the roll angle ϕ (rotation along the y axis), and the Plunge (End-effector Z position to respect to the base). The reference system considered is shown in Fig.3-5 with the letter D.

3-2-5 Canfield joint reliability

NASA Glenn Research Center, in the pre-paper [11], analyzed the kinematic workspace of the Canfield Joint and discovered that this kind of gimbal has great workspace robustness since if one of the motors at the base fails and it is no longer possible to control that motor angle, the mechanism is still able to show great maneuverability as shown in Fig.3-6

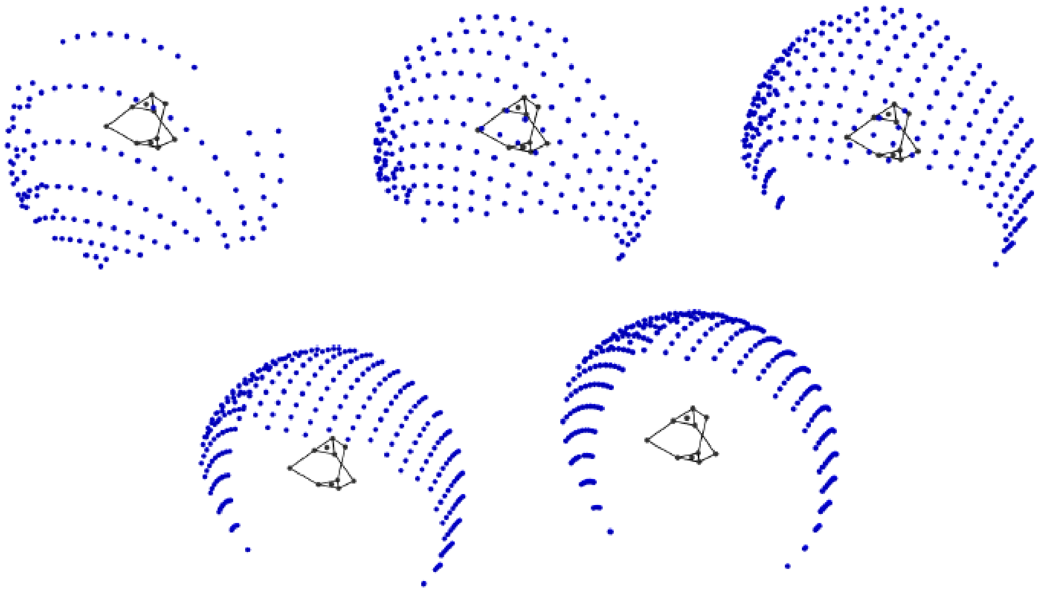

Figure 3-6: Visualizations of the workspace of the center of the distal plate in the event that is fixed. From left to right, we have: Top: $\theta = 80°$; $100°$; $120°$. Bottom: $\theta = 140°$; and $160°$. [11]

To allow the exploitation of this feature of the mechanism explained in this study, a Reinforcement learning (RL) code will be proposed for future implementation in the section 11-1. All the Kinematics and control will be replaced by the RL model that will first learn to control the kinematic structure through training in the nominal condition. The model will later be trained in the failure condition in which one of the motors is blocked in a fixed position. The model by training in this new working condition will learn how to control the two remaining motors to achieve a correct pointing in the new allowed workspace produced by the off-nominal condition.

3-3 Pointing systems on the market

Since the CubeSat market for deep space application is in rapid development, the current availability of a small pointing mechanism necessary to allow data transfer for long-distance application is not fully developed yet.

The main current competitors a parallel pointing mechanism are:

- Tethers Unlimited
- Comat agora

Tethers with the COBRA™-HPX [12], developed a parallel pointing mechanism, with a very compact stowed footprint of 115 mm.

Comat Agora on the other side is a European company that developed the TRIPOD [13] that is based on a similar design but has a bigger size since is not developed for CubeSat.

Both of them are sold with their respective controller and kinematic algorithm but no data is given in respect to the tracking algorithm system and in the case of the COBRA™-HPX the company guarantees a maximum life span of two years.

Since in Argotec's Andromeda project the minimum recommended life span needed is of 5 years and since the development of such a system would be prominent in all future lunar and deep space missions, a high number of this system will be required in this growing market. For this reason, a new design concept will be developed in this thesis to developed a system based on the Carpal wrist designed by Dr. StephenCanfield [6], but within mind high mechanical and control reliability, production scalable with low production costs, and maintenance free.

In section 9 the innovation keys between the existing pointing mechanism market for small satellite and the developed design will be analyzed.

Chapter 4

Configuration Trade-off

4-1 Primary mechanical design

With the rigid constraints correlated with the available space destined to the pointing mechanism, two preliminary designs were developed that were able the produce a structure that has to be contained in an envelope op 115mm of diameter, with structural rigidity, and capable to sustain the dynamical loads exerted to the structure in the launching phase.
After a presentation of the possible design configurations, a trade-off analysis will be made between the two.

4-2 2-axis pointing mechanism design

Within mind the idea that "the best design is the simplest design" since in a simple design there are fewer components that could fail, the first hypothesis of a pointing mechanism was made considering a 2-axis structure. In most applications, conventional 2-axis gimbal systems are preferred since these are mechanically simple and the control of these gimbal typology is well documented and straightforward, so a 2 axis architecture was developed for the first design iteration.

This design consists of two motors controlling respectively the Azimuth and the Altitude of the pointing mechanism. In the stowed configuration the height of the antenna is used to optimize the motor position to allow a wide range of motion in the deployed configuration since the rotational joint (controlling the altitude) is placed higher in respect to the gimbal base.

However, there are some chronic problems associated with a two-axis configuration. One of those is the fact that the cabling equipment usually imposes restrictions on the gimbal movements, and to overcome this problem, slip rings or rotary unions should be used. This equipment is attached to the rotational axis to allow electricity (power and data) to be

Figure 4-1: Stowed configuration first design version

Figure 4-2: Deployed configuration first design version

transferred from a stationary part to the moving part while allowing full turn continuous motion.

Furthermore, while this structure shows a wide range of motion and a very compact stowed configuration, the gimbal presents a big aluminum support structure needed to guarantee high rigidity that has a negative impact on the mass budget of the satellite. Moreover, this design is not safe since there is not much space to put redundancies to be able to make the system resilient in case of a motor failure.

For these reasons, the analysis moved toward a system that presents a more articulated structure, but at the same time checked all the needed characteristics for the pointing mechanism while maintaining a high level of fidelity and safety.

4-3 Carpal wrist based design

In the second iteration, the design took inspiration from the Canfield Joint design since, as discussed in section 3-2-4, this kind of design can guarantee a very compact stowed configuration, taking advantage of the extra Dof called Plunge that allows the gimbal to control its Z position, and allowing a high dexterity and pointing capabilities.

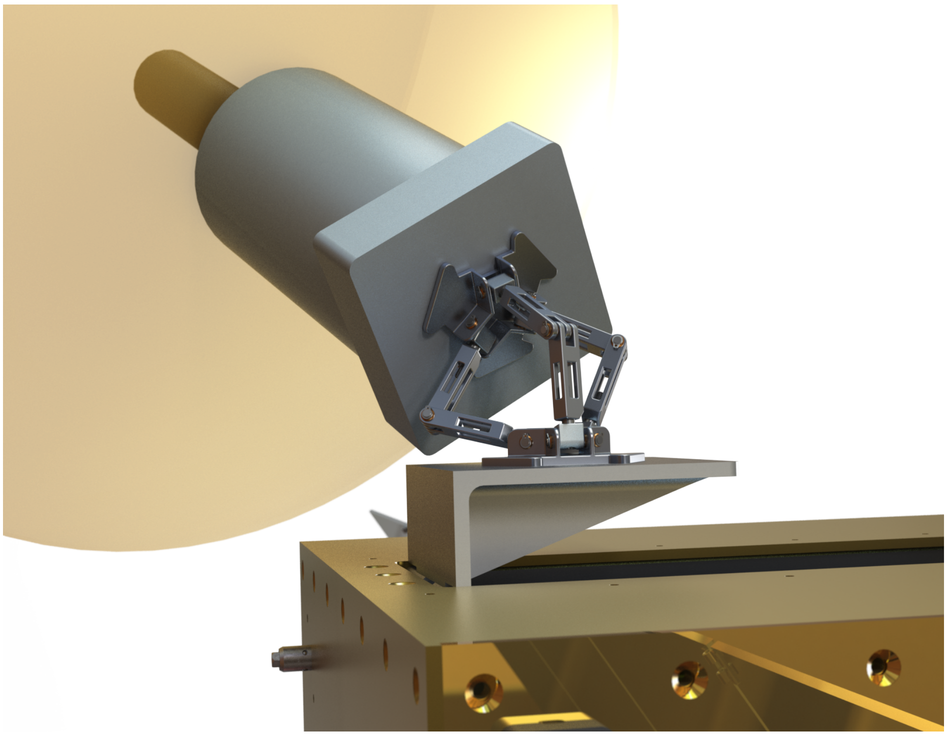

Figure 4-3: Modular design version mounted on satellite

The first iteration of the parallel pointing mechanism was designed with modularity and production costs in mind since all the parts of the arms are designed to be obtained from a single part easy to manufacture with a common two and a half axis CNC machine. This allows the gimbal to be able to be mass-produced to guarantee the feasibility of the coverage for big satellite constellation usage.

The pointing mechanism is composed of three main parts:

- The sub-part of the arm
- The Base and platform
- The connecting hinge

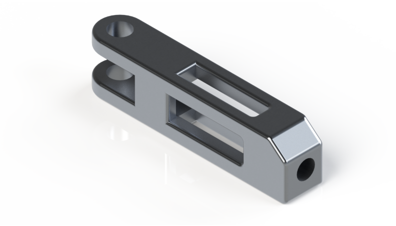

Figure 4-4: Arm sub-part

Figure 4-5: Base

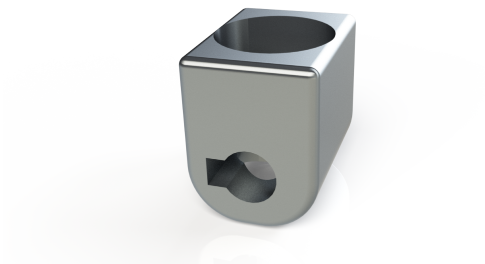

Figure 4-6: Hinge

Those parts are design to be assembled together using standard hardware, the components are:

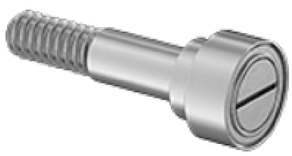

Figure 4-7: Track Roller

Figure 4-8: Sleeve Washer

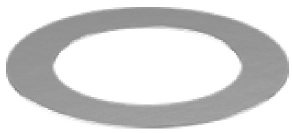

Figure 4-9: Ring Shim

Figure 4-10: Elbow Shafts

Those components are assembled together as shown in Fig-4-11 and in Fig.4-12.

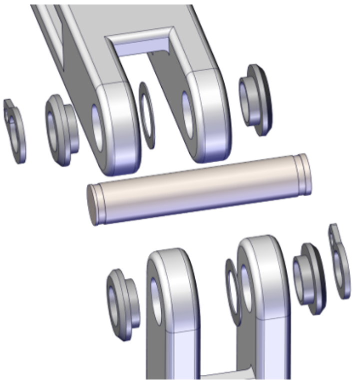

Figure 4-11: Elbow connection

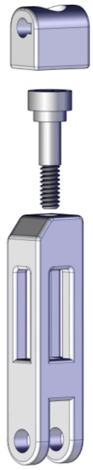

Figure 4-12: Hinge to arm connection

The gimbal arms were designed in such a way to allow an angle of up to 160 deg to be reached in the deployed configuration. This mechanical safety feature allows the gimbal to have a reset position in which the manipulator can go in case of a malfunction of a motor or a position sensor and at the same time it is mechanical protection against the singularity zone of the workspace. This mechanical stoppage is composed of a bulge that goes in contact with a transverse element placed on the opposite arm subsystem as shown in Fig.4-13.

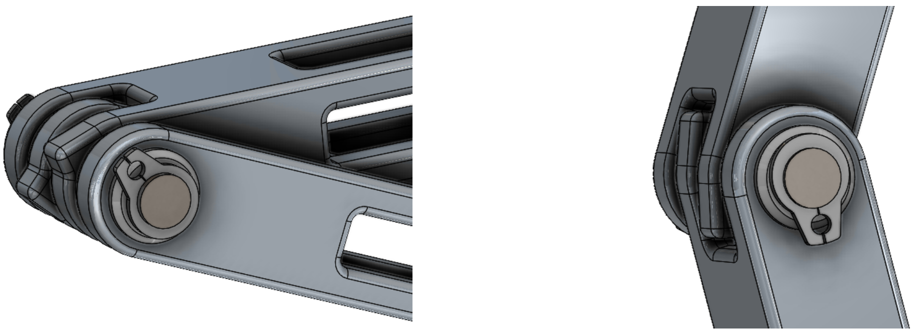

Figure 4-13: Elbow mechanical safety feature

Both the Stowed and deployed configuration are shown respectively in Fig.4-14 and Fig.4-15 where the maximum reachable platform height is visible.

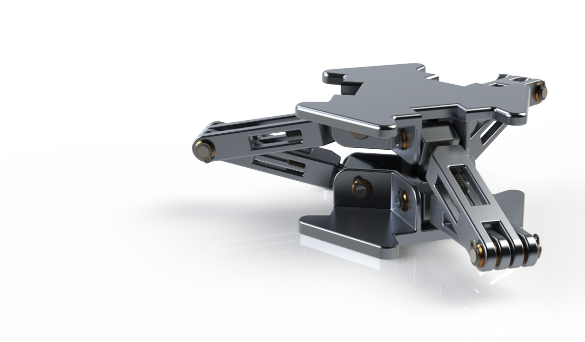

Figure 4-14: Stowed configuration

Figure 4-15: Deployed configuration

The dimensions of the gimbal were imposed to allow the stowed gimbal configuration to be fully enclosed in a 1 U domain (100 x 100 x 100 mm) as shown in Fig.8-5.

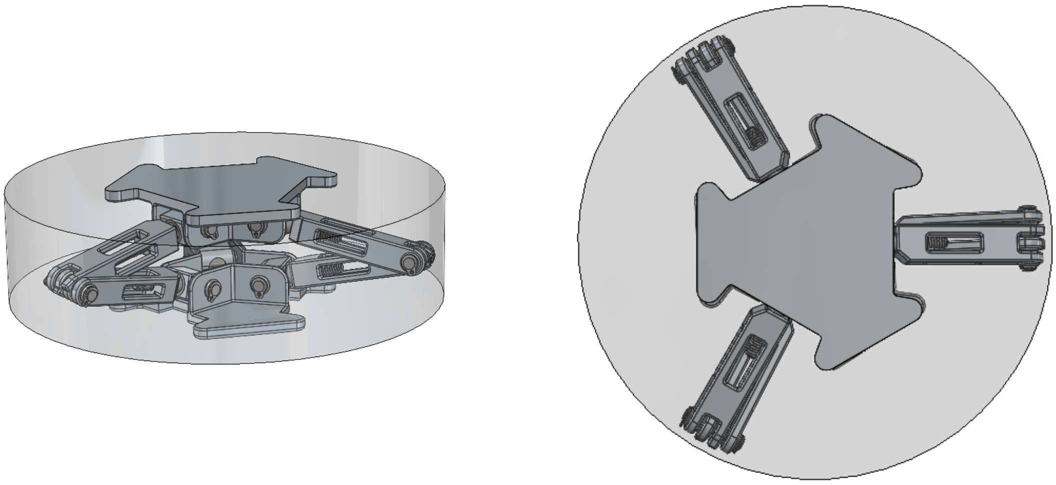

Figure 4-16: Stowed configuration envelope

Further analyses on the optimal dimensions of the platform/base and arms will be discussed in section 6-4 where, through the use of a dynamical simulation of the pointing mechanism, the geometry was optimized to achieve a geometry capable of minimizing the motor torques needed to allow the necessary pointing capabilities. So the preliminary set of dimensions of the various components were set to be able to proceed with the kinematic study of the structure.

4-4 Trade off

The main advantages and disadvantages of the two design configurations are reported and the final configuration selection will be explained.

4-4-1 2-axis pointing mechanism

The main advantages of this design are:

- Control simplicity
- Compact stowed configuration
- Wide pointing domain

On the other hand, the drawbacks are:

- Cable management complexity
- No redundant safety systems

4-4-2 Carpal wrist design

The main advantages of this design are:

- Rigid and light structure
- High pointing accuracy
- Compact stowed configuration
- Wide pointing domain
- Failproof (Paper NASA)
- Internal cable protection

On the other hand the drawbacks are:

- Control complexity
- Mechanical complexity

4-4-3 Trade off result

Because of the preview points, for the specific application, the carpal wrist-based design was preferred to the 2-axis because of its cable management capability, and because it has great workspace robustness since if one of the motors at the base fails the mechanism is still able to show great maneuverability as discussed in section 3-2-5.

Chapter 5

Kinematic analysis of mechanism

As for all robotic mechanisms, a Kinematic study is crucial to be able to study the motion of the structure. Since the fundamental task of a robot is to position and orient a tool in a specific manner, a mathematical model of the particular manipulator must be developed to provide the necessary control of the device.

Robot manipulators are composed of links that are connected by joints, which can be revolute (rotating) joints or prismatic (linear), that allows the structure to orient itself in the desired position [14]. To be able to fully orient a rigid body in space, a six degrees of freedom manipulator is needed to control the tree position and the tree orientation of the tool.

After the kinematic analysis is done, an equation of motion is obtained which is unique to the physical device.

To obtain this model it is necessary to find a mathematical function relating the input position parameters to the output position parameters and the goal of the function is to describe the forward and inverse position relationship in closed form.

There are two distinct kind of kinematics:

- Forward kinematics Forward Kinematics (FK)
- Inverse kinematics Inverse kinematics (IK)

FK allows to figure out the position and orientation of any point of the robot by knowing the joint position. On the other hand IK works symmetrically, by knowing the position and orientation of the robot end-effector we can obtain the various robot joints angles necessary to reach the desired position.
In our application, we know the desired antenna orientation and we want to know the required joint position necessary to reach that orientation. For this reason, there will be extended use of the IK.

5-1 Solving Inverse Kinematics

There are two main ways to solve IK:

- Analytic solution
- Numerical solution

The analytic solution means that you can derive, in closed-form, an expression for the joint positions given the desired end-effector position. This is beneficial because all the work is done offline and solving the IK will be fast, on the other hand in the case of a manipulator which has redundant degrees of freedom there can be multiple analytic solutions that can produce the desired position.

So in many cases, the numerical solution is preferred. This one is generally slower and less predictable than an analytic solution but they can solve harder problems. This method is based on the use of an optimization algorithm that has the task of minimizing the pointing error between the actual and desired position of the manipulator. That is why this method is preferred in the case of complex manipulators since there is no need of deriving the mathematical equation that describes the manipulator position.

The kinematic study was first done with a mono-dimensional model and later the study was extended to a more complex three-dimensional model to be able to include friction and torques for a more accurate dynamic study.

5-2 Mono dimensional elements analysis – RIGID BODY TREE method

The rigid body tree robot model is a MATLAB tool that is used to represent a manipulator through the use of linear mono-dimensional elements and joints. The structure is made of rigid bodies that are attached via joints. Each rigid body has a joint that defines how that body moves relative to its parent in the tree.

This tool is capable of controlling just linear manipulators, but this limitation was bypassed by constructing the gimbal as three separated linear arms (Fig.5-1) and imposing geometric distance constraints between the arms extremities (Fig. 5-2) since in the gimbal those are all connected to the platform.

In this phase, the training of the inverse kinematics is been done with twenty training iterations. The higher the number of training iterations, the smaller the error will be between the desired and actual position.

Imposing the 3 position and 3 rotations of the end-effector, the robot by solving Analytical inverse kinematics returns the angles (in radians) of all the revolute joint necessary to reach the desired position and returns the final visual configuration.

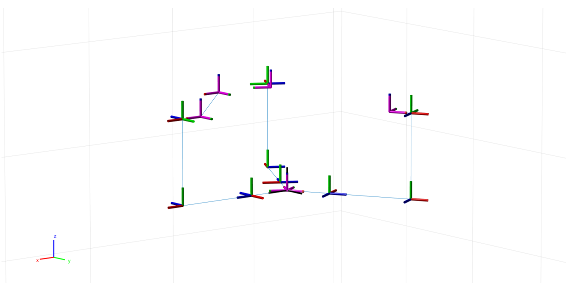

Figure 5-1: Open rigid body tree structure

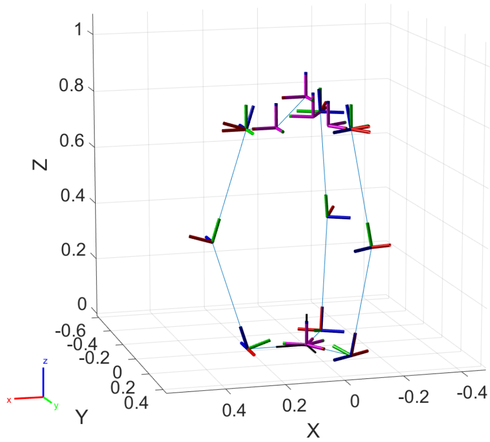

Figure 5-2: Final assembled structure

As an example the combination of input data and obtain gimbal configuration is shown in Fig.5-3.

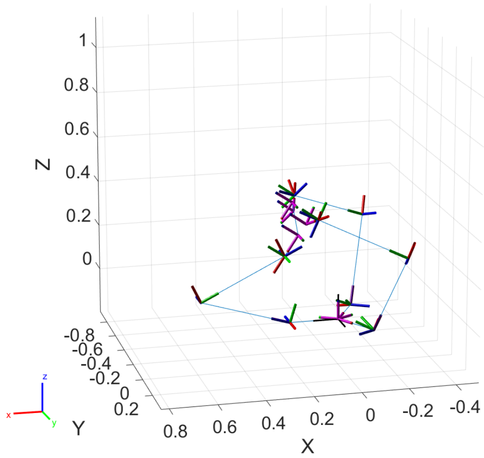


```
%End effector desired position
X=0;
Y=0;
Z=0.65;

%End effector desired orientation
Rx=0;
Ry=pi/3;
Rz=0;

%posizione e direzione dell'endEffector

poseTgt3.TargetTransform = trvec2tform([X, Y, Z])* eul2tform([Rx Ry Rz]);
```

Figure 5-3: 60 deg Y orientation gimbal configuration

5-2-1 Trajectory following code

The mono-dimensional model was further expanded by developing a trajectory following code that allows producing a continuous trajectory by interpolating a set of way-points with a third-order equation.

Trajectory thus obtained was then discretized in a series of steps that were used as frames. For each frame, the inverse kinematics was solved and the immediately previous step was used as starting position for the following one. In this way, the code was able to generate a set of commands that allows the machine to follow the required imposed trajectory. The resulting trajectory is shown in Fig.5-4.

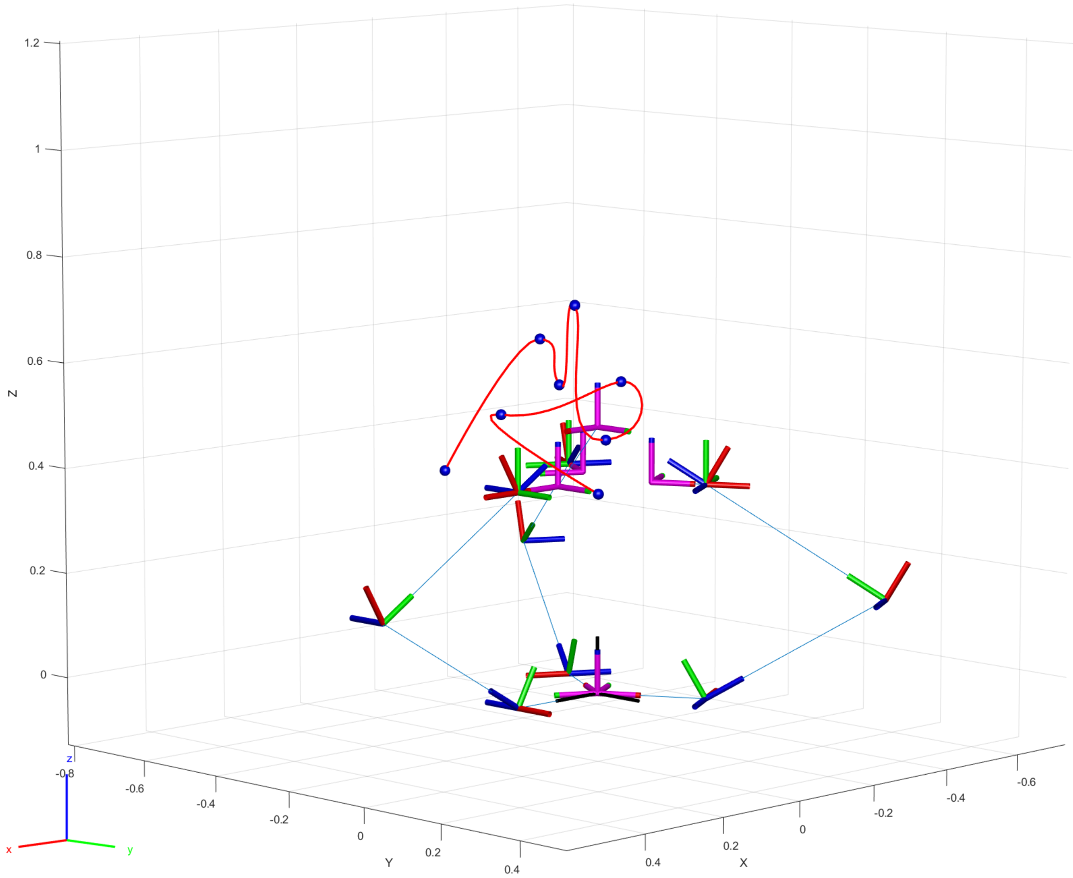

Figure 5-4: Trajectory following code

5-2-2 Mono-dimensional elements limitations

At this stage, the correct functioning of the kinematics of the pointing mechanism was proven, but this mono-dimensional model showed also its limitation.

Since it was written in MATLAB™ environment it was not able to treat time in the same way a simulation does and its simplicity did non allow the implementation of more complex physical dynamical phenomenon such as torques required, inertia, friction, and mechanical wear of the internal components.

To allow those further analysis, a new model was constructed using the Simulink environment by utilizing the MATLAB™ connection to allow the construction of a parametric model that allowed an optimization study of the gimbal dimensions, chapter 6-4.

Chapter 6

MATLAB - Simulink model

Since the main goal of this thesis is to study the behavior of the designed pointing mechanism in the final lunar environment and to determine mechanical components and dimensions capable to guarantee the required task, a more sophisticated simulation of the mechanism was developed using MATLAB™ - Simulink.

Simulink, through the use of the Simscape Multibody toolbox (used to assemble the structure) and by utilizing the direct MATLAB™ connection (used to calculate the inverse e forward kinematics), can simulate the behavior of a robot in a particular set environment to analyze its behavior Fig.6-1.

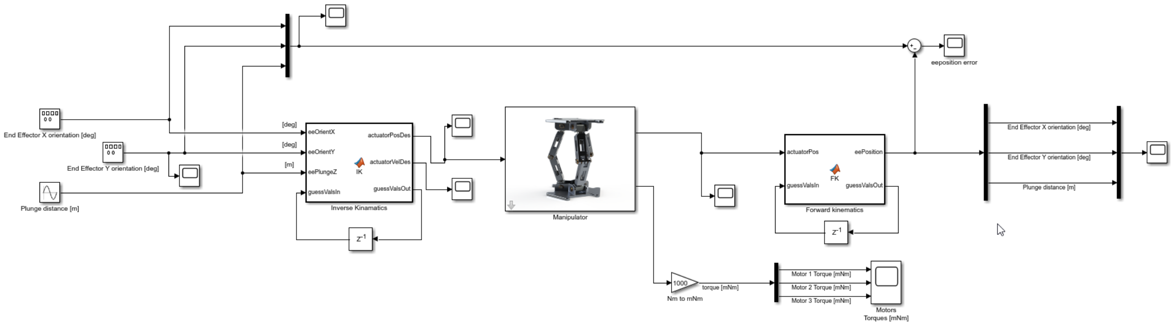

Figure 6-1: Simulink model

The model consists of a "Manipulator block", in which the gimbal is mechanically defined with all the rigid parts and the interaction between them through revolute joints, and two Matlab functions blocks in which inverse and forward codes are contained.

6-1 Manipulator block

The manipulator block has the main aim of constructing the gimbal by defining the solid parts, the system coordinates translation and rotation between all the parts, and the joint types required between the solids 6-2.

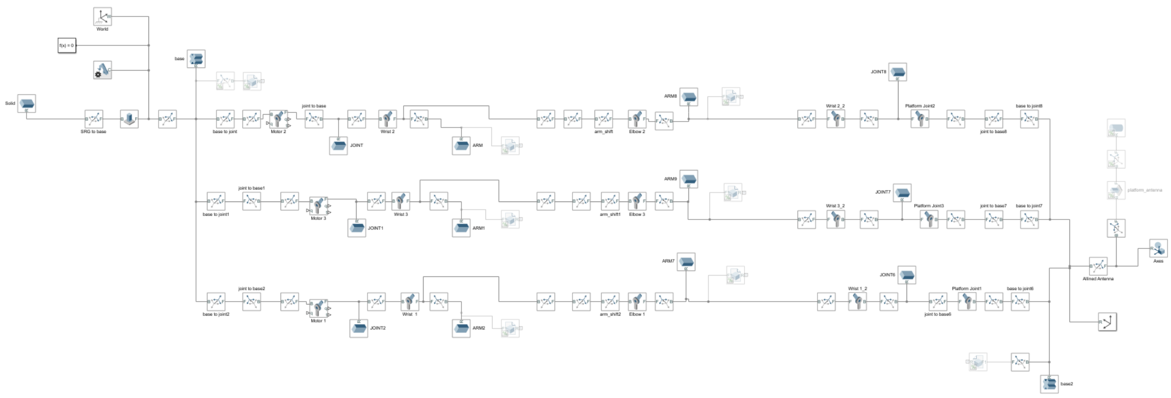

Figure 6-2: Manipulator block

The initial design was obtained with simple geometries (Brick solids for the arms and wrists, and extruded equilateral triangles for the base and platform) to allow faster simulation time while maintaining the correct behavior and dimension of the actual gimbal.

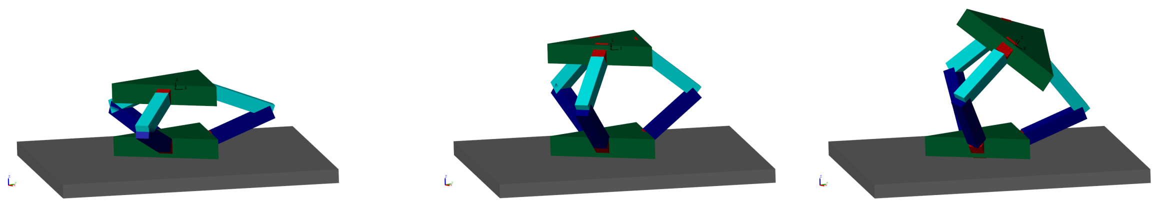

Figure 6-3: Simple gimbal movement

The simplified geometry allows the structure to be easily modified since it is constructed through parametric code and to find the optimized dimensions, chapter 6-4, that at the same time allows the motor torques minimization and the maximum dexterity and wide non-singularity domain. The final optimized geometry data was then used to design the final structure in CAD 3D and imported back into the Simulink model replacing the simplified blocks to allow to simulation to take into account the inertia matrices and mass of the actual parts, section 7.

The bock contains also the motor backlash data that will be critical in the PID controller tuning section, section 7, and the damping coefficient of the joints that was set to a preliminary value of $0.001\frac{N*m}{deg/s}$. This preliminary value will later be experimentally estimated through hardware in the loop simulation in which the desired position of the joints will be compared with the actually reached position through the use of an encoder placed on the joint axis.

6-2 IK and FK blocks

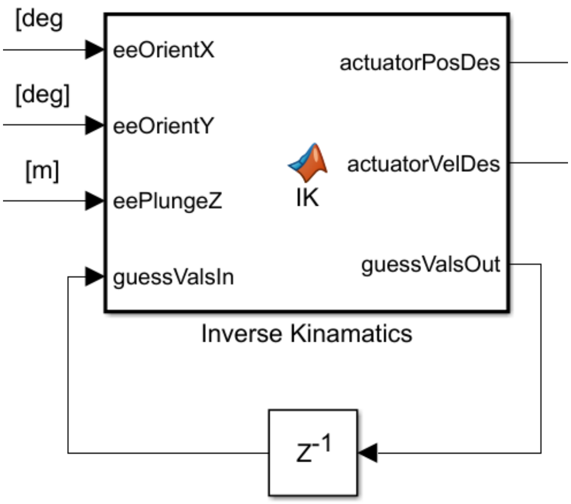

Figure 6-4: IK MATLAB function

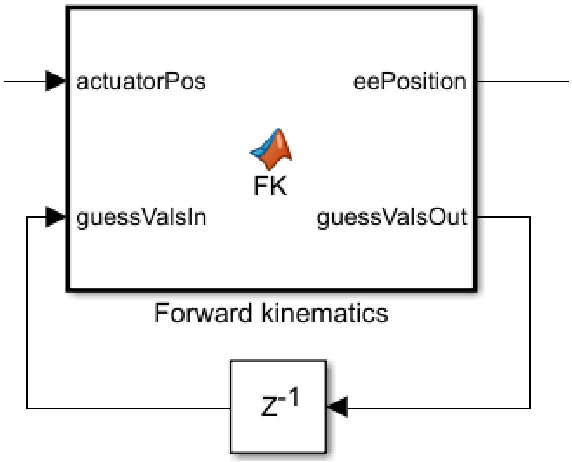

Figure 6-5: FK MATLAB function

The "brain" of the simulation is contained in the two blocks shown in Fig.6-4 and Fig.6-5. As shown in Fig.6-4 the IK block receives as input the two orientations of the gimbal (rotation around the X and Y axis) and the Z height of the platform, called Plunge [6], and the previous output configuration as the initial guess for the following step to be developed.

The input data could be any kind of external signal or trajectory data to be followed, but in this case was set to a sinusoidal signal of $30deg$ amplitude and $0.5rad/s$ of frequency for the X orientation and $0.7rad/s$ for the Y orientation, Table6-1. The third Degree of freedom (Dof) (the Plunge) was set to a custom pattern to allow to gimbal to deploy from the stowed configuration and then to follow a controlled height change during the two rotation controls as shown in Fig.6-8.

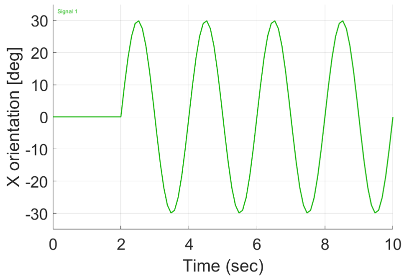

Figure 6-6: X orientation plot [deg]

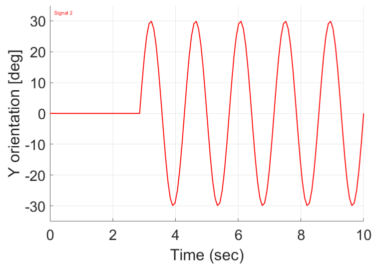

Figure 6-7: Y orientation plot [deg]

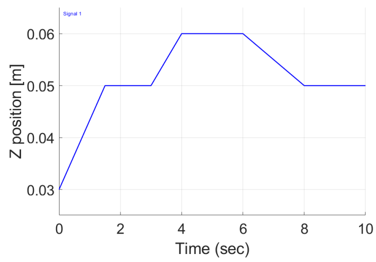

Figure 6-8: Z position plot [m]

On the other hand, the outputs of the IK block are the instantaneous motor's position required to reach the desired position and the motor velocities to reach it in the desired step size.

Table 6-1: End effector motion input data

Controlled Dof	Frequency [Hz]	Amplitude [deg]	Start at [s]
X Axis orientation signal	0.5	30	2
Y Axis orientation signal	0.7	30	2.85

The Plunge position was set to a custom pattern to allow to gimbal to deploy from the stowed configuration and then to follow a controlled height change during the two rotation controls as shown in Fig.6-8.

The FK, shown in Fig.6-5, is used to check the positioning error of the model to validate it. It receives the real position from the actual joint encoder and through a forward kinematics code, it establishes the end-effector position.
By comparing the input end effector position-orientation signals with the actual end-effector position we can establish the IK block error, shown in Fig.6-9. Since the maximum error on the end effector orientation is in the order of 10^-7 deg the model can be considered valid, Table.6-2.

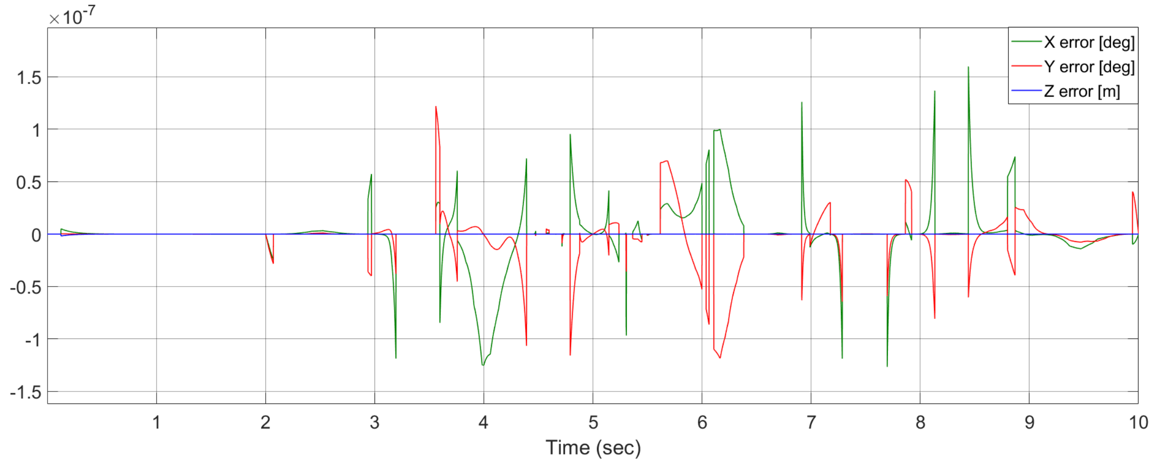

Figure 6-9: IK end effector error plot for the three controlled Dof

Table 6-2: Peak end effector position error data

Peak error	Value	Time [s]
X Axis rotation	$1.59 * 10^{-7}$[deg]	8.44
Y Axis rotation	$1.22 * 10^{-7}$[deg]	3.56
Plunge	$4.88 * 10^{-11}$[m]	6.11

6-3 Sensitivity analysis

Now that a valid model was developed a sensitivity analysis was performed to analyze the correlation between the selected parameters and the motor torques and shows the parameters that have the biggest influence on the motor torque required to allow the needed movement. From this analysis, we can determine the best design strategy to follow to obtain the optimum geometry for our use case.

The parameters that were analyzed in the sensitivity analysis were:

- The lower arm length
- The upper arm length
- The base and platform radius

For all the tree parameters, a range of maximum allowable value and the minimum value was set and uniform distribution of possible intermediate values was imposed for the arm length and for the base radius since the whole range of the spectrum was equally allowed.
The Parameters and the distribution range of the analysis are shown in Table6-3.

Table 6-3: Sensitivity analysis parameters

Parameter	Distribution	Min. Value	Max. Value
Lower arm length [m]	Uniform	0.045	0.085
Upper arm length [m]	Uniform	0.045	0.085
Base radius [m]	Uniform	0.028	0.060

From the scatter plot shown in Fig.6-10, a series of 50 designs were automatically produced from the combination of the probability distribution values that the three parameters can reach.

Every blue point in Fig.6-10 represents an individual design and for each of them, a simulation was run with the end-effector position presented in section 6-2 as input. The simulation can output the torque value required for each joint that allows the gimbal to move in the desired position with the set speed, as shown in Fig.6-11.

By comparing the Torque values obtain from the fifty designs we can obtain a plot (Fig.6-12) that shows the correlation between the tree parameters and the torque value.

The sensitivity analysis shows that all the three variables are directly proportional to the motor torques, but the major contributor of the torque is the platform size ($base_r$) and the lower arm length (arm_h). On the other hand, the upper arm does not have a big impact on the torque values. So to be able to obtain a structure with a wide working volume, and at the same time low torques, a gimbal with long arms and a small platform should be preferred. In the optimization phase 6-4, we will so focus on a geometry with long enough arms to allow a big working domain, but at the same time a platform and arms light enough to maintain the inertia low.

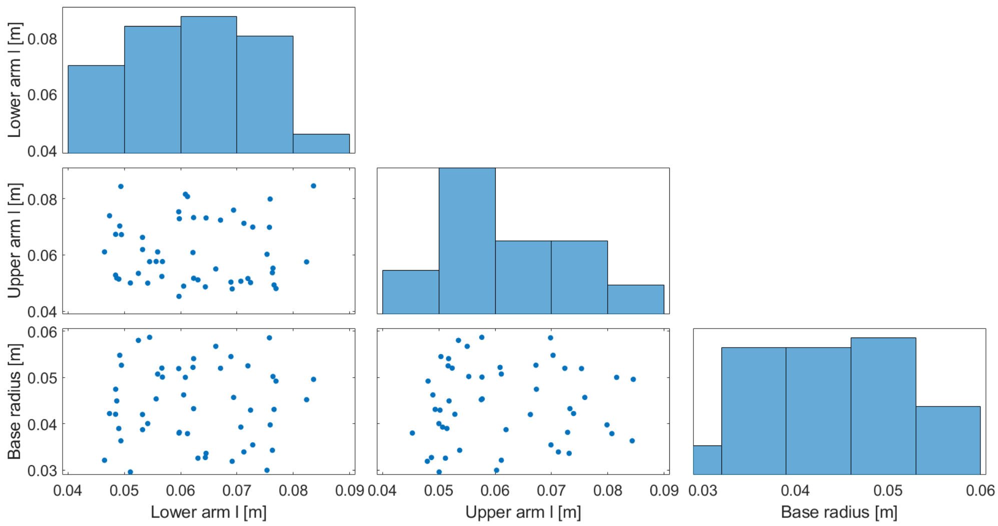

Figure 6-10: Scatter plot

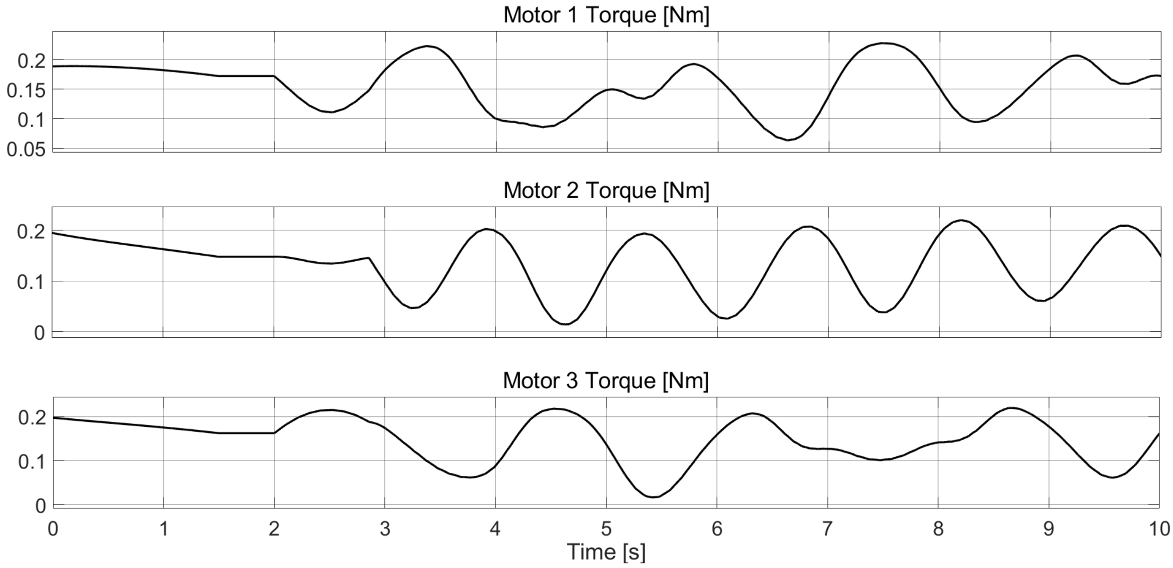

Figure 6-11: Motors torque in 1g condition

6-4 Structure optimization

From the data acquired from the sensitivity analysis, a geometry optimization of the structure was performed to determine the dimensions that would at the same time:

- Maintain a compact stowed envelope
- Minimize the maximum torques

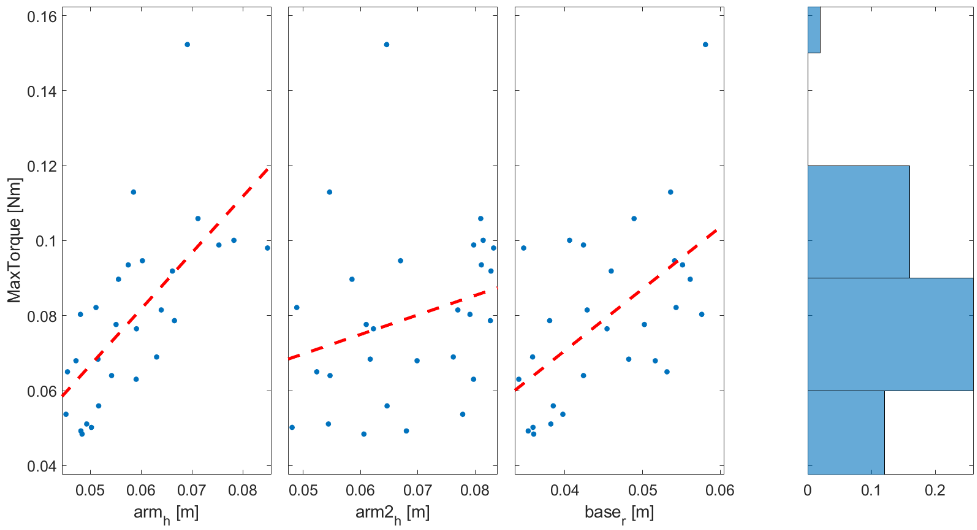

Figure 6-12: Sensitivity analysis with trend lines

The optimization requirements, parameters and results are discussed in section6-4-1.

The optimization method that has been chosen is the Gradient descent Method which is a local optimization technique that returns only the local minimum of a function by tweaking iteratively its parameters. It all starts by defining the initial parameter's values and from there gradient descent uses calculus to iteratively adjust the values so they minimize the given cost-function [15]. It all starts with a multi-variable function $F(x)$ that represents the motor torques distribution related to a particular combination of the selected editable parameters. If $F(x)$ is defined and differentiable in a neighborhood of a point a, then $F(x)$ decreases faster if the point a moves in the direction of the negative gradient of F at a, or in mathematical terms:

$$a_{n+1} = a_n - \gamma \Delta F(a_n) \tag{6-1}$$

Where $\gamma \Delta F(a_n)$, with $\gamma \in R_+$, defines the step size taken to reach the minimum.

so with a suitable step size, we obtain:

$$F(a_n) \geq F(a_{n+1}) \tag{6-2}$$

By setting an initial guess value, if the step size is suited for the specific case, we will obtain a monotone decreasing sequence Eq.6-2.

This optimization method was selected since it is a fast optimization technique that has the only downside that, like all local optimization methods, requires a good initial guess for the parameters. As shown in Fig.6-14, the initial guess values can bring the optimization solution to a different local minimum, but since in this gimbal the design geometry is quite defined and fixed by all the design thresholds needed to obtain a compact stowed configuration able to be contained in the satellite, it is perfectly suited for this application.

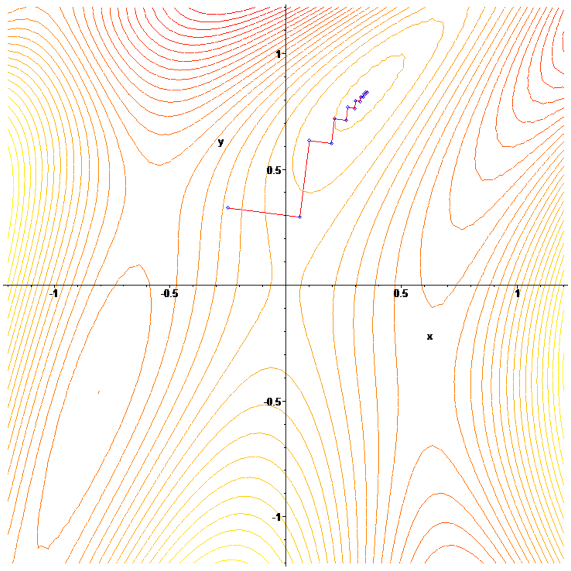

Figure 6-13: Gradient descent algorithm in action

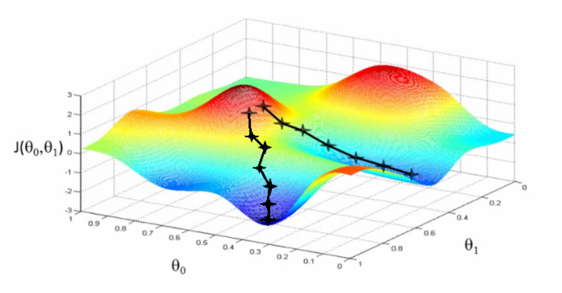

Figure 6-14: Importance of the first guess value

6-4-1 Optimization Results

The optimization started from initial guessed values. In combination with the guess value, a range of allowable dimensions was chosen to localize the optimization process in a range of values that allow the gimbal to be manufacturable. Those values and the ranges are shown in Table6-4.

Table 6-4: Optimization parameters

Parameter	Initial set Value	Min. Value	Max. Value
Lower arm length [m]	0.068	0.050	0.070
Upper arm length [m]	0.068	0.050	0.085
Base radius [m]	0.032	0.030	0.045

It can be seen how the ranges are more centered to the desired value compared to the values selected for the sensitivity analysis 6-3. This allows the optimization to be faster and to be directed to the best local minimum, as discussed in section6-4.

The optimization algorithm produced a random set of parameters combinations (Fig.8-14) and outputs the max torque value. It finds by iteration the direction of the negative gradient and follows the new parameter combination obtain until it finds the local optimization minimum, as shown in Fig.6-16.

While the upper arms have a lower impact on the motor's torque values compared to the rest of the parameters and a higher upper arm length would allow a broader domain of motion control, it was chosen to maintain the acceptable range value on the smallest dimensional range allowed as was done with the sensitivity analysis.

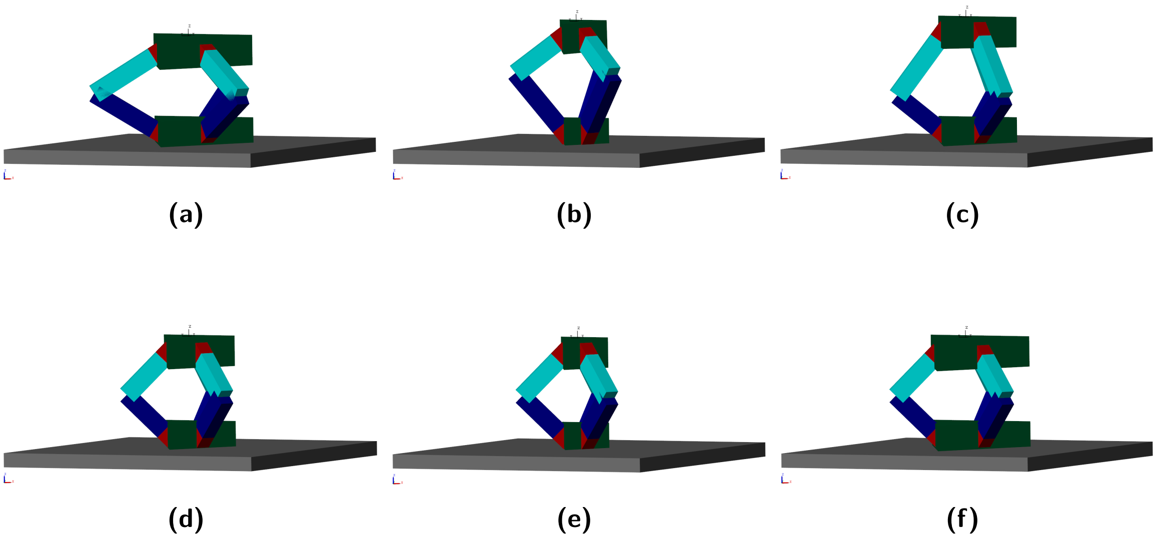

Figure 6-15: Randomized parameters combination generation for simulation

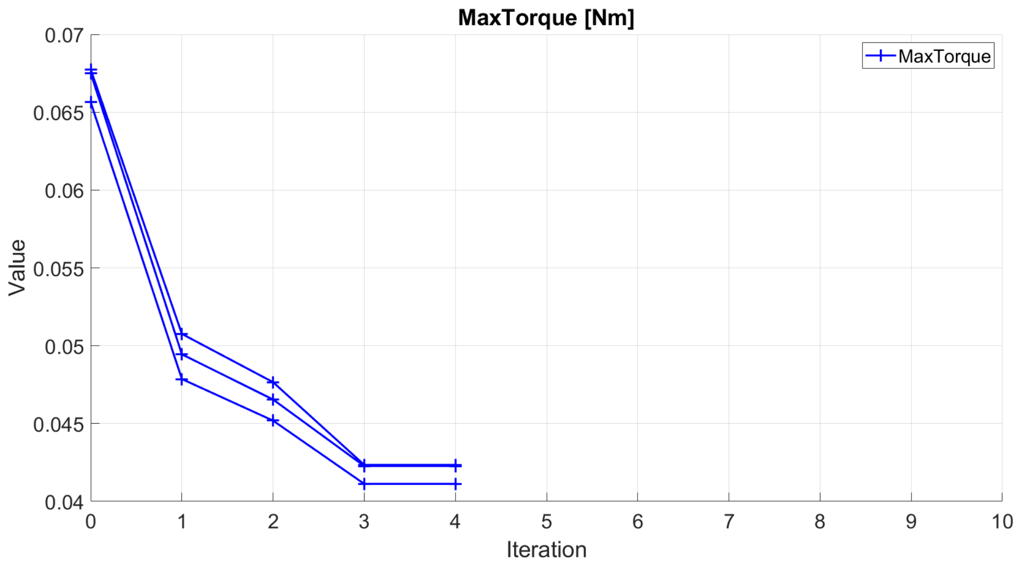

(a)

Figure 6-16: Max.Torque optimization

In this way the geometry optimization algorithm has the possibility of obtaining a structure with the same upper and lower arm length, as shown in Tab.6-4, since the simulation shows that with different arm length the kinematic tends to present a wider singularity zone.

For this reason and to obtain a more compact stowed configuration, the final optimized design has the dimensions shown in the table 6-5.

The torque improvement and the stowed radius requirement that had to be met, are shown respectively in Fig.6-16 and Fig.6-17.

Table 6-5: Optimization results

Parameter	Final optimized Value
Lower arm length [m]	0.050
Upper arm length [m]	0.050
Base radius [m]	0.030

The dimensions refer to the design (e) of Fig.8-14.

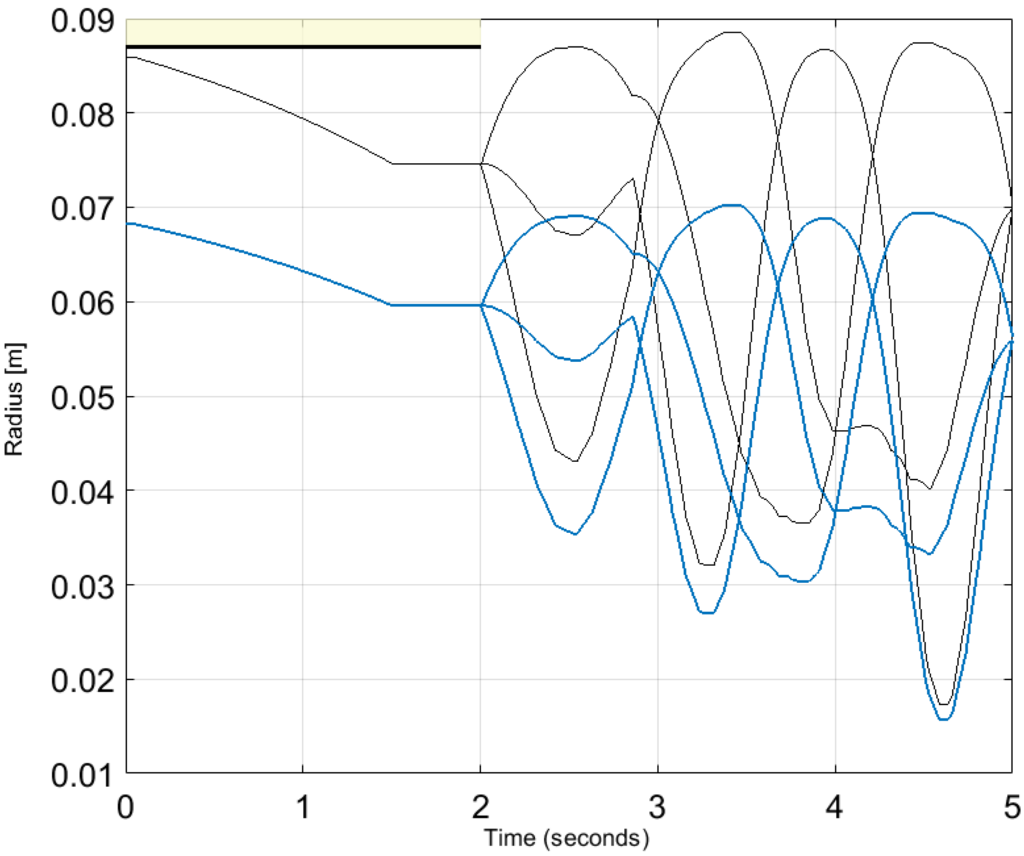

(a)

Figure 6-17: Comparison between the initial maximum envelope radius data and the after optimization radius data

The final mechanical structure can be designed with the values obtained from the optimization process and the final geometry is shown in section 8.

6-4-2 Hypothesis

All the preview dimensions were referred to the prototype dimensions, which is a scaled version of the final flight model. The prototype was chosen to be scaled since the main task of the gimbal prototype is to test the motion controller algorithm developed and a bigger structure reduces the hardware costs, in particular the motor price.

The feasibility of the flight model was demonstrated with a dynamic simulation in which the final size geometry was set and the simulation was run in a 0g environment with a cylindrical mass that simulates the High gain antenna mounted on the gimbal platform as shown in Fig.6-18.

The motor outputs are shown in Fig.6-19 and with this data, a preliminary motor able to guarantee the needed torque and speed was selected. The motor is DC brushless with low maintenance and with a 70% margin on the torque value required to produce the desired motion.

The torques and the datasheet of the chosen motor are shown in Fig.6-20.

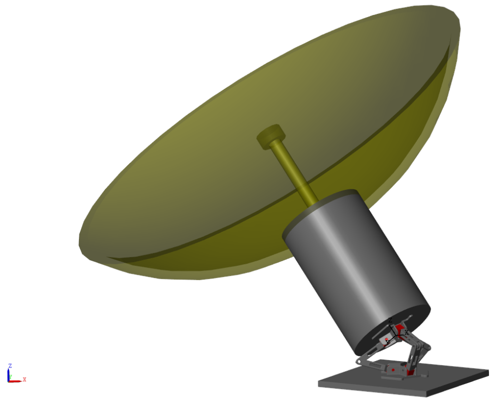

(a)

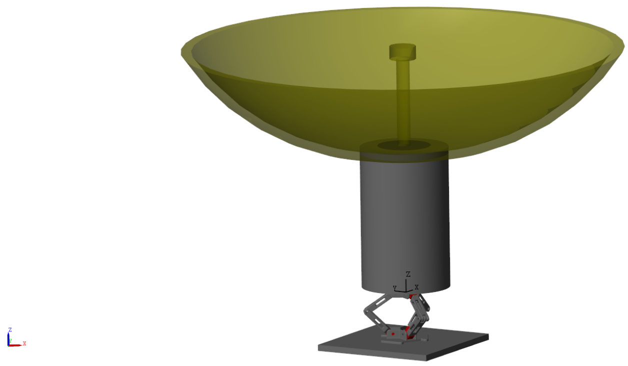

(b)

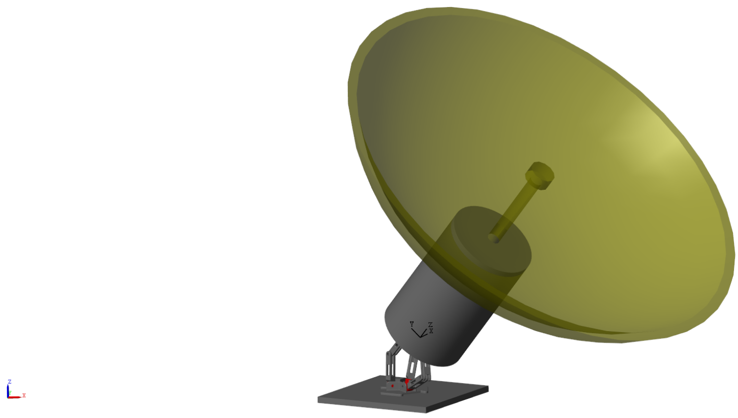

(c)

Figure 6-18: Animation of flight model simulation in zero g condition

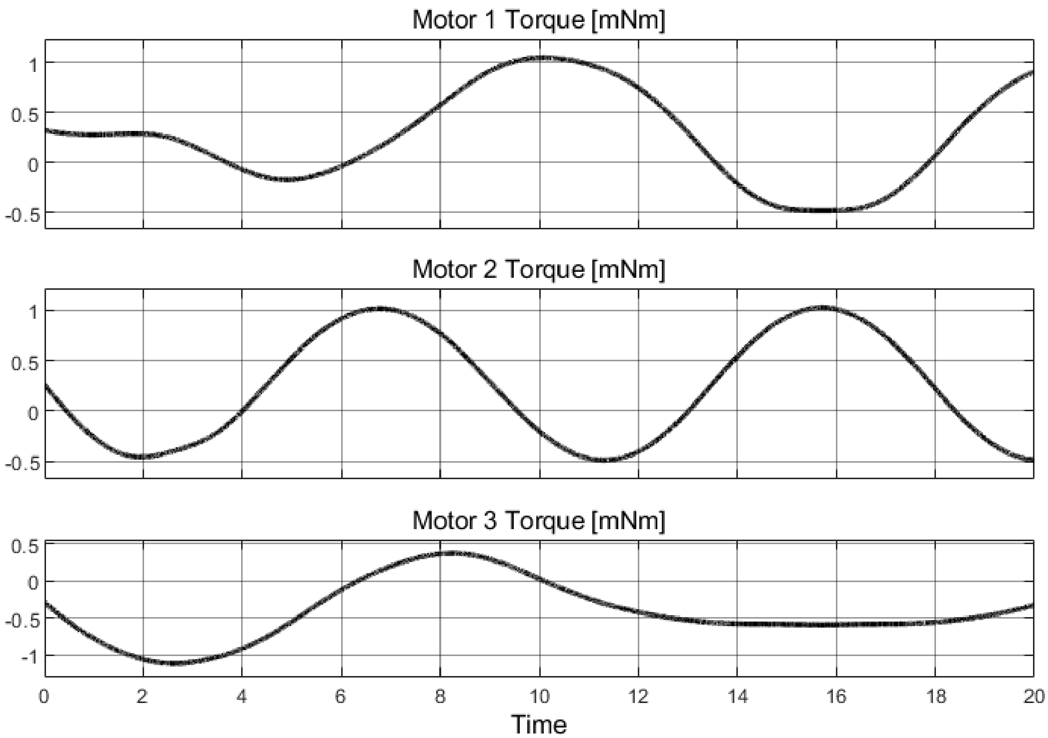

Figure 6-19: Flight version motor torques

VALUES AT NOMINAL VOLTAGE	
Nominal voltage	6 V
No load speed	49200 rpm
No load current	160 mA
Nominal speed	41700 rpm
Nominal torque (max. continuous torque)	1.74 mNm
Nominal current (max. continuous current)	1.66 A
Stall torque	12 mNm
Stall current	10.4 A
Max. efficiency	77 %

Figure 6-20: Selected motor specs

Chapter 7

Dynamics and Control

The main scope of the Dynamics analysis is to map the required joint forces and torques to their position, velocity, and acceleration [16].

To move from kinematics to dynamics, we need more information about the manipulator's mechanics. Specifically, we need the following inertial properties:

- Mass:
  Newton's second law relates mass to force and linear acceleration.
- Inertia:
  This is a 3×3 matrix, commonly called the inertia tensor, relating torque and angular acceleration. Since this matrix is skew-symmetric, it can be defined with 6 parameters:
  - 3 diagonal elements, or moments of inertia, which relate torque about an axis with acceleration about that same axis.
  - 3 off-diagonal elements, or products of inertia, which relate torque about an axis with acceleration about the other two axes.
- Center of mass:
  If the center of mass is not located at the body coordinate frame we defined, we need to apply the parallel axis theorem to convert the rotations about the center of mass to rotations about our coordinate frame of interest.

All of this data is obtained from the final CAD obtained from the previous sections. The gimbal sub-parts were output in *cgr* format (CATIA file) to be received back to Matlab. The *cgr* format contains the geometry of the part and its inertial matrix data. With this information the simplified blocks used in the preliminary Simulink simulation explained in section6 can be further analyzed from a dynamical point of view.

In combination with the density data, which is visible in Table 7-1, Simulink can determine the true torques required to move the gimbal in the desired way as described by the IK block

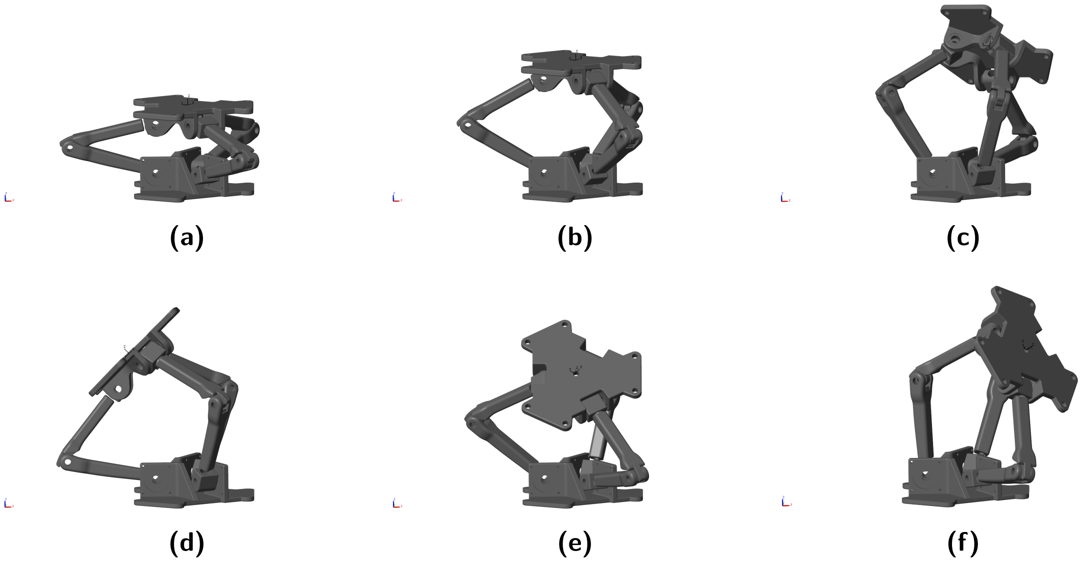

Figure 7-1: Simulink motion analysis performed on the final mechanical design

input data.

As shown in Table 7-1, two main materials were chosen for the gimbal design. The ABS plastic will be used for the first prototype, which has the aim to verify the kinematic controller and correct movements of the gimbal. The Aluminum 7075 on the other hand will be used for the Ground model (GM) version of the gimbal to test the thermal behavior of the system and test the long-lasting life of the mechanism.

Table 7-1: Material proprieties

Material	**Tensile Strength [MPa]**	**Thermal Coefficient of expansion** $[10^{-6}]$	**Density [g/cm3]**
ABS (resin 3D printed)	50	80	1.05
Al 7075 T6	500	23,5	2,80

As an example of the data which is calculated for every single part of the gimbal, the ABS 3d printed upper arm data are shown in Table 7-2.

Table 7-2: Upper arm CAD derived data

Propriety	**Value**
Mass [kg]	0.0084
Center of mass position $[m]$	[-0.00478269, -0.0289461, 0.00900013]
Moment of inertia $[kg * m^2]$	[3.25145e-06, 1.96623e-07, 3.22126e-06]
Product of inertia $[kg * m^2]$	[-1.28435e-11, -1.61534e-12, -4.85487e-08]

In the following section 7-1 an introduction of the motor selection and control characteristics is discussed

7-1 Controller and motor selection

A trade of analysis was first made to decide which motor was preferable for the specific application. The main required characteristics of the motor are:

- Zero maintenance long life spectrum
- High torque and low speed
- Compact geometry

For all these reasons the trade-off felt between a brushless motor and a stepper motor. Since the motion needed is just 180 deg the perfect choice would have been a servo motor because of its simplicity, but it is incompatible with the long-lasting life requirement because of the mechanical contact between the internal parts.

In the following sections, accurate analysis of the two motor type advantages and disadvantages will be determined with the development of two respective control actuation logic.

7-1-1 C.C. Brushless motor design configuration

The main advantages of the brushless motor are:

- No mechanical contact between internal parts
- High reliability

The disadvantages are:

- High-speed application (for this reason it would require a gear motor reduction system that adds complexity and moving parts to the system)
- Control noise risk in the space environment

This kind of motor requires a power-based controller that outputs a set current to the motor concerning the relative desired and actual motor position. For this reason, as shown in Fig.7-2, the actual position is obtained from an encoder and its signal is fed back to the controller. In the controller block, this signal is compared to the desired position and this error is fed into a PID that generates an output that commands the simulated motor shown in Fig. 7-3.

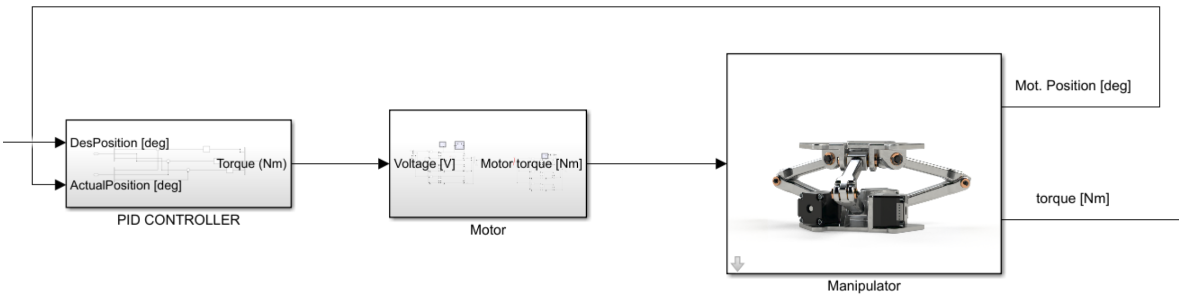

Figure 7-2: Simulink blocks logic used to control the Brushless motor

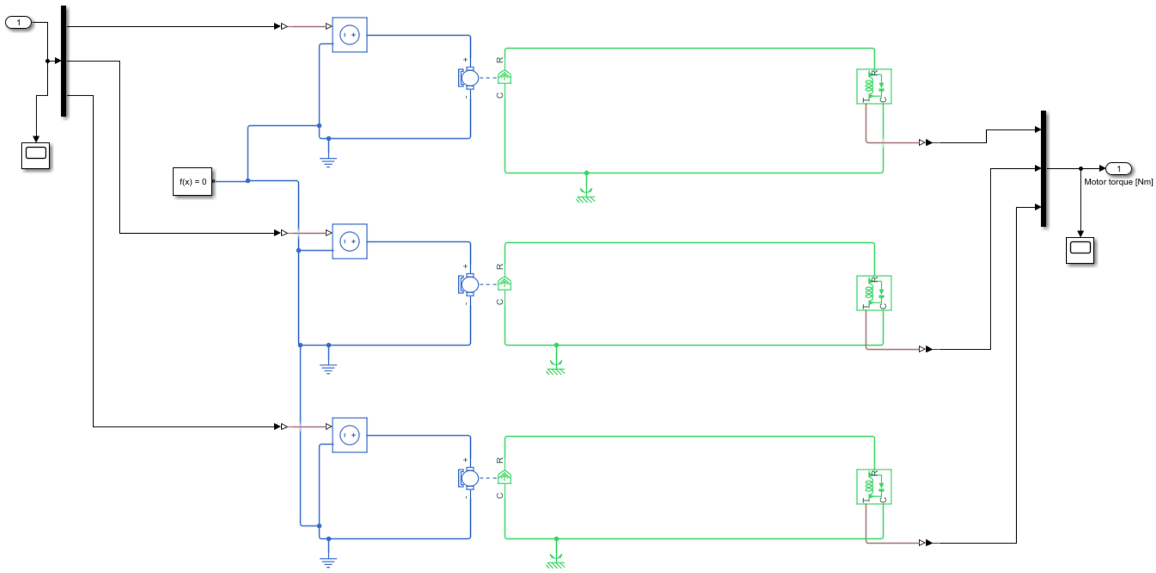

Figure 7-3: Electrical circuit used to command the brushless motor

In the motor block, the signal received from the PID controller is used as a controlled voltage source that powers the motor. In the simulation a torque value is extracted from the motor block to be fed to the multi-body simulation explained in section 6.

From the explained simulation to a precise torque value of each motor could be extracted and the simulation results are shown in Fig. 7-4 and Table 7-3.

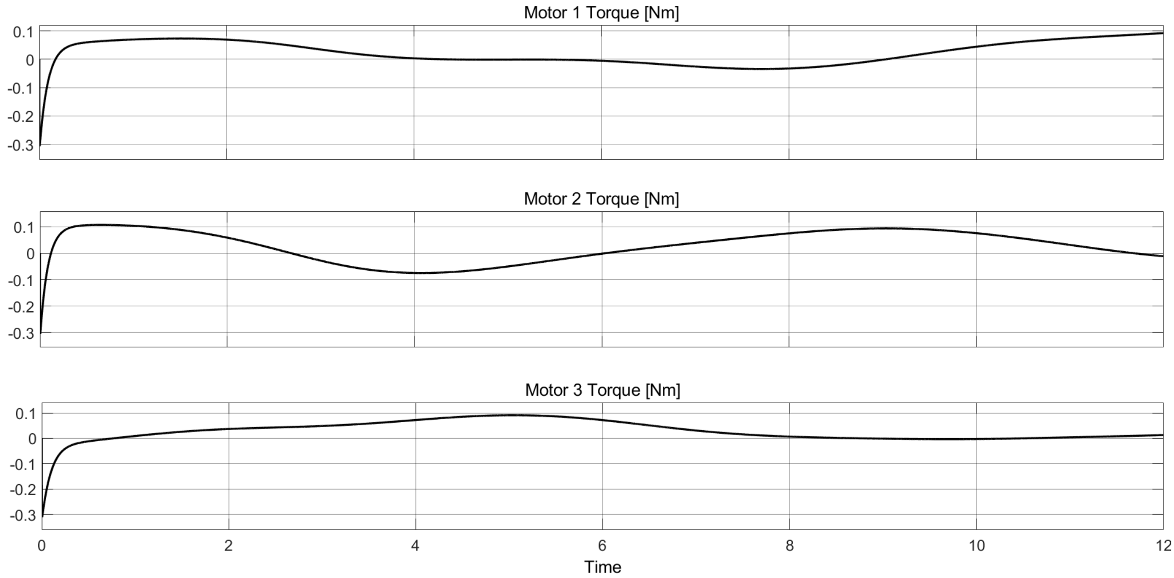

Figure 7-4: Simulation output torques required for the brushless motor

Table 7-3: Brushless motor max torque

Peak Torque	Value	Time [s]
Motor 1	$7.34 * 10^{-2}$[Nm]	1.51
Motor 2	$1.07 * 10^{-1}$[Nm]	0.65
Motor 3	$9.09 * 10^{-2}$[Nm]	5.05

This first control hypothesis was later left out in favor of a stepper motor design and the characteristics that support this choice will be discussed in section 7-1-2.

7-1-2 Stepper motor design configuration

The stepper motor was the final design choice for the gimbal prototype.

The main advantages of the stepper motor are:

- No mechanical contact between internal parts
- No need for a gear motor reduction system
- High capability of maintaining the motor position

On the other hand, the disadvantages are:

- Control noise risk in the space environment
- limited capability of high-resolution angle control

Since the stepper motor works in a different logic compared to the Brushless motor, a new simulation structure was designed to determine the torque and other motor characteristics that are required to allow the desired motion.

The motor block shown in Fig.7-2 was replaced with a new subsystem that presents inside three stepper motor as shown in Fig.7-5

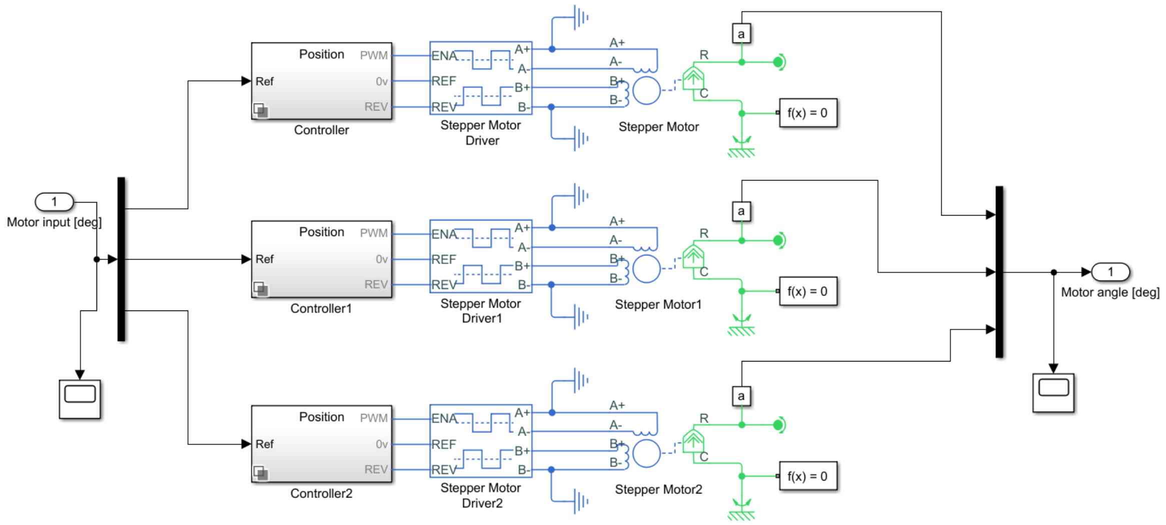

Figure 7-5: Electrical circuit used to command the stepper motor

Each stepper receives as input the desired position that he has to reach, the shaft is connected to a motion sensor (contained in the block "a") that measures the actual achieved position and sends that position signal to the Multibody manipulator block.

To allow the simulation to be more realistic and to allow the controller to be tested in a non-ideal environment, a new block called *Backlash* shown in Fig.7-6 is inserted. This block considers the presents of mechanical play inside the motor structure that is always present in the real hardware and therefore tests the controller more realistically. The backlash value will be tuned to the exact value during the hardware in the loop testing in which the optical encoder, mounted to the back of the motor will measure when the actual desired position is reached and send to the stepper motor controller the signal to send further step positions to compensate for the mechanical play or to correct the torque levels required to allow movement which can be greater than the ideally expected one.

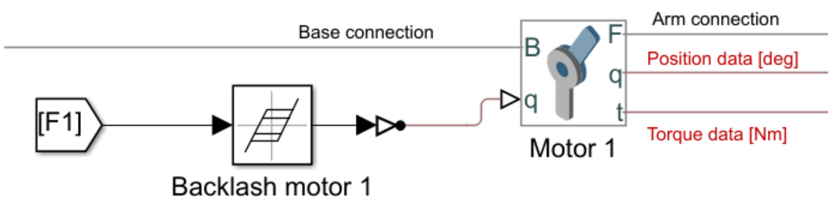

Figure 7-6: Backlash block that considers the motor imperfection data inside the simulation

Chapter 8

Mechanical design

Now that the final optimized dimensions of the gimbal are been determined through the kinematic analysis and the motor type and size was selected through the dynamical analysis, the final mechanical design was developed.

8-1 Design inspiration

The previous modular design had the drawback that the arms had to be shifted apart to allow the use of a single-arm subpart, but this creates an asymmetry in the structure that could result in a non-uniform stress distribution on the arm shaft and consequently uneven wear of the bushings. So an alternative arm design was developed taking inspiration from the human elbow to maintain the protective mechanical protection discussed in section 4-3.

Exactly as in our mechanism application, in the human arm the bone structure, through evolution developed in a way that allows 90 degrees of rotation in one axis, while giving stability and rigidity in the fully extended configuration through the Olecranon, curved bony eminence of the ulna that projects behind the elbow shown in Fig.8-3.

By following the Biomimicry philosophy, which is the practice that learns from and mimics the strategies found in nature to solve human design challenges, the arm it's been designed as 2 separated parts imitating respectively the femur and the combination of radio end ulna composition. A protuberance was placed in the upper part of the mechanical arm to simulate the Olecranon.

Furthermore, the two arms are complementary to each other, as for the meeting surface present between the Capitulum and the Trochlea with the Fovea shown in Fig.8-4, to allow a further level of safety allowing the kinematic to work even in case of mechanical wear of the primary meeting surfaces.

With this design, we obtain a structure that (is not as cheap and easy to manufacture as the modular version but) has a higher mass to strength ratio, is more reliable, compact, and is

Figure 8-1: Final mechanical design

symmetric.

In the following chapter, the criteria and methods that are been used to obtain the geometry of the structure will be explained.

8-2 Platform Design topological optimization

From the sensitivity analysis results, explained in section 6-12, it was apparent how the motor torques are directly proportional to the platform size. This is because with a bigger platform, the inertia of the platform increases, and with that the inertial forces that the motors have to compensate to allow the desired movement.

For this reason, to optimize the mechanical design it would be convenient to minimize the platform mass.

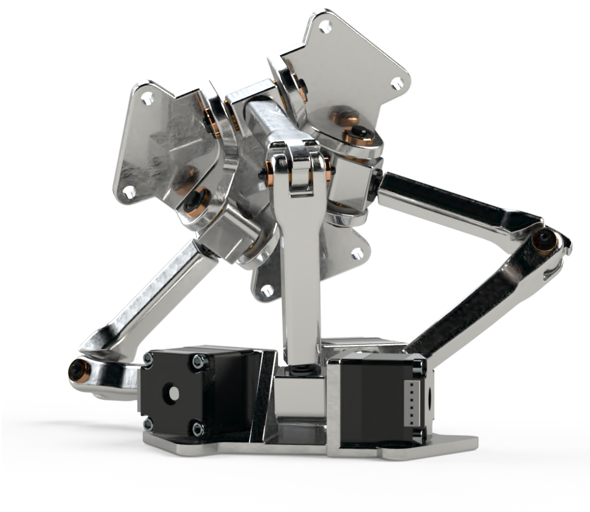

Figure 8-2: Gimbal arms structure

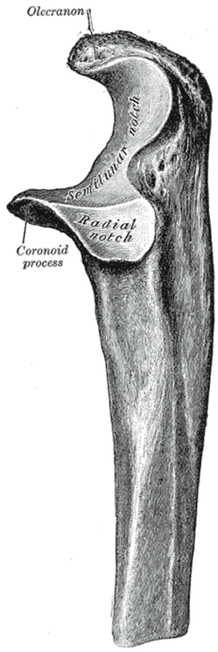

Figure 8-3: Human elbow bone

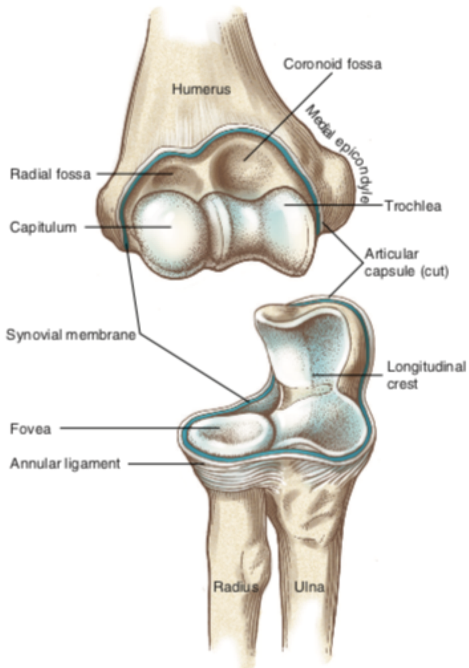

Figure 8-4: Contact surfaces in the bone structure

Figure 8-5: Gimbal elbow detail

To minimize the mass a topological study was performed.

The topological optimization was done in two load scenarios:

- Load orthogonal to the platform surface
- Load parallel to the platform surface

The two analysis are analyzed in two sections and from them, a final design is obtained.

8-2-1 Orthogonal load case optimization

This load configuration can simulate the deployment load condition and all the gimbal plunge movement. The initial design which is used as the domain for the optimization is shown in Fig.8-6.

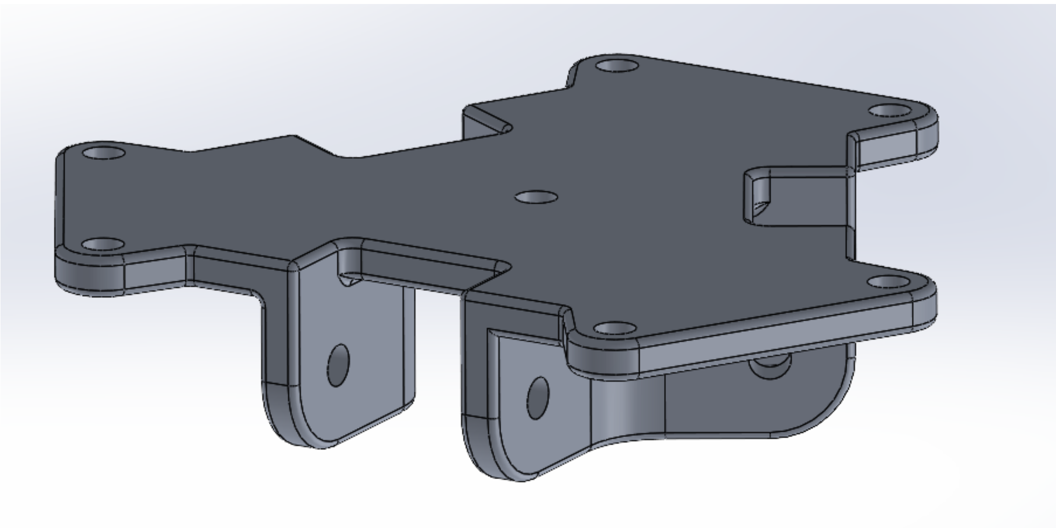

Figure 8-6: Pre optimized model used as the topological optimization 3D domain

The axial load is placed in the positive Z end effector direction applied on the fixing holes since in this way all the lower part of the platform is subjected to a $\sigma > 0$ state of tension which is worst possible load condition that the platform needs to be able to handle. The load constraints are a pinned joint fixture and two simply supported hinges placed on the holes that connect the platform to the arms.
Both the loads and the constraints are shown respectively in purple and green in Fig.8-7.

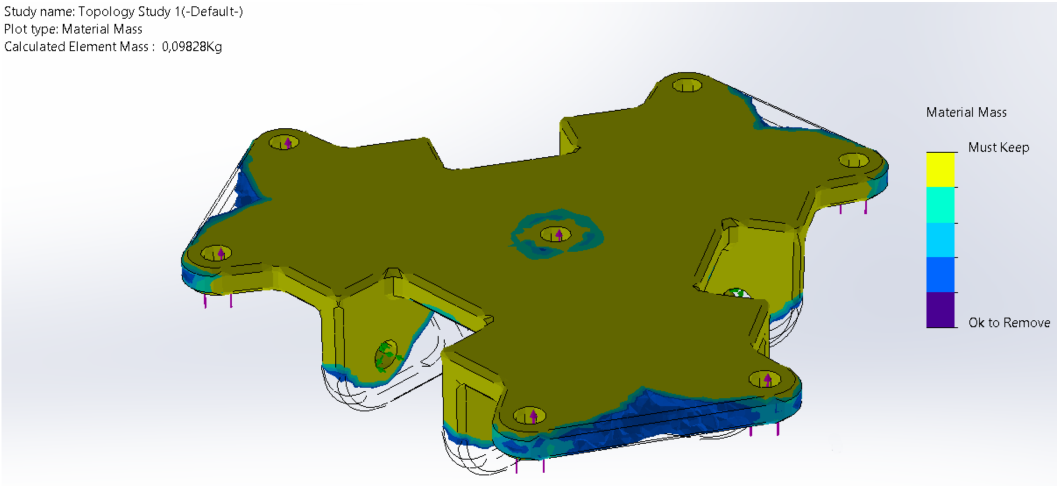

Figure 8-7: Orthogonal loads (purple) and fixing constrains (green) used for the topology study

The resulted optimized structure, 35% lighter than the original design is shown in Fig.8-8.

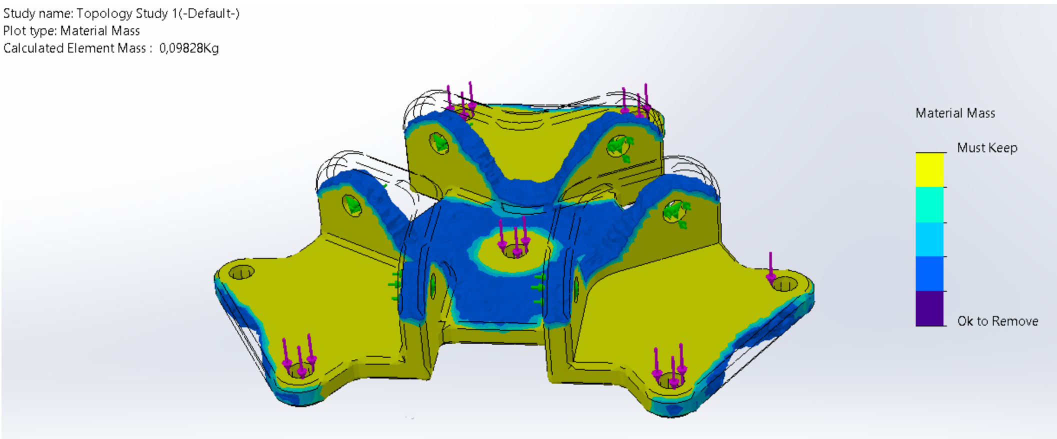

Figure 8-8: Orthogonal loads optimization results

8-2-2 Parallel load optimization

The parallel load configuration is used to test the condition in which the platform is placed in a 90 deg configuration with respect to the base.

The configuration load is set as a displaced load set at a distance equal to the Centre of gravity (CoG) position of the antenna assembly in respect to the platform surface.

The constraints are the same as in the Orthogonal load case 8-2-1.

Both the loads and the constraints are shown respectively in purple and green in Fig.8-9.

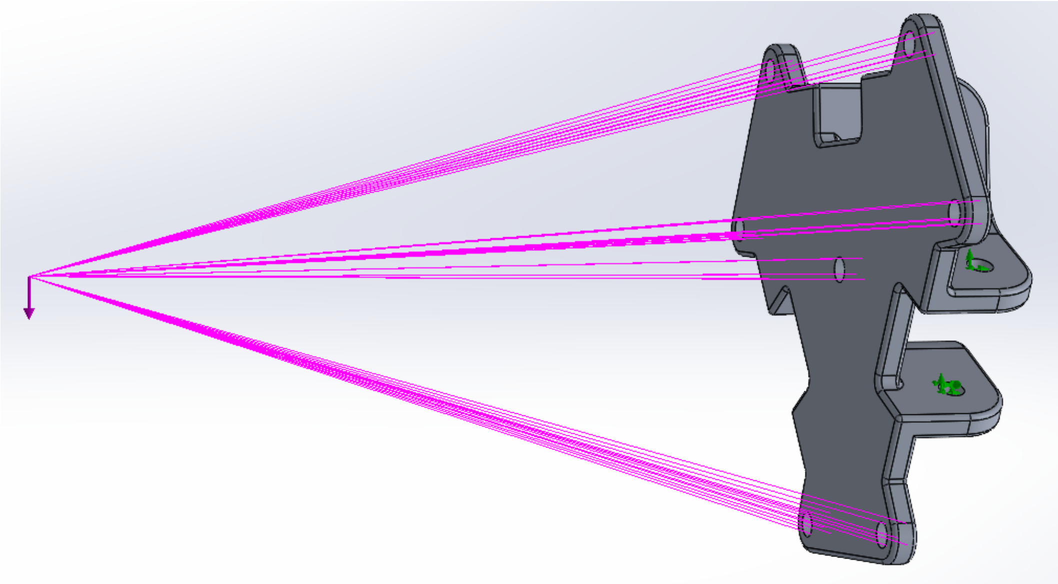

Figure 8-9: Lateral loads (purple) and fixing constrains (green) used for the topology study

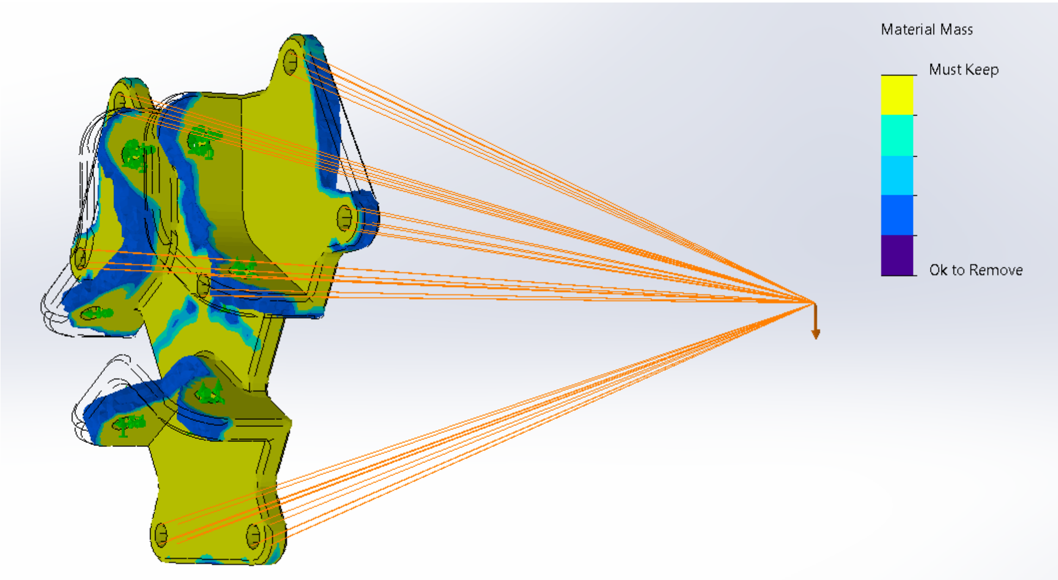

Figure 8-10: Lateral loads optimization results

Also in this configuration, the target final mass was set to an optimized value of 35% mass reduction.

8-2-3 The final obtained geometry

From section 8-2-1 and section 8-2-2 it is visible that the final lightened design in both load cases has a similar geometry.

The topological optimization code outputs a mesh that was used as a base to construct a new platform design. The final geometry is shown in Fig.8-11.

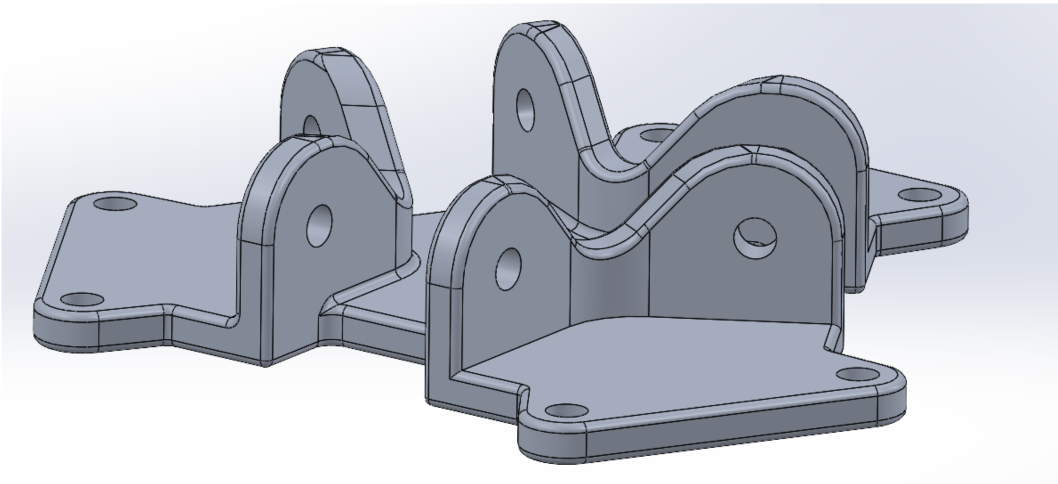

Figure 8-11: Optimized inspired final platform design

8-3 Mechanical joint design

Now that the power source of the gimbal has been developed, to focus moved toward the design of the various joints of the gimbal.

One of the first consideration that was done was that, since the motion speed of the various parts will be very low (Maximum 5°/s) in the gimbal design bearings will not be used since they insert an extra level of possible failure points and the speed and loads that the bearing should be able to hold in the zero-g environment are not sufficient to justify the choice.

Instead, self-lubricating bushings (Fig.8-14d) will be used for their simplicity, high load support capability, and low maintenance need. On the other hand, the joint that connects the motor to the arm (shown in Fig.8-12 and Fig.8-13) will present an angular contact ball bearing (Fig.8-14b) in the prototype model to allow the Degree of freedom (Dof) needed to allow the axial rotation of the arm and at the same time support the axial load that the platform will transfer to the base.

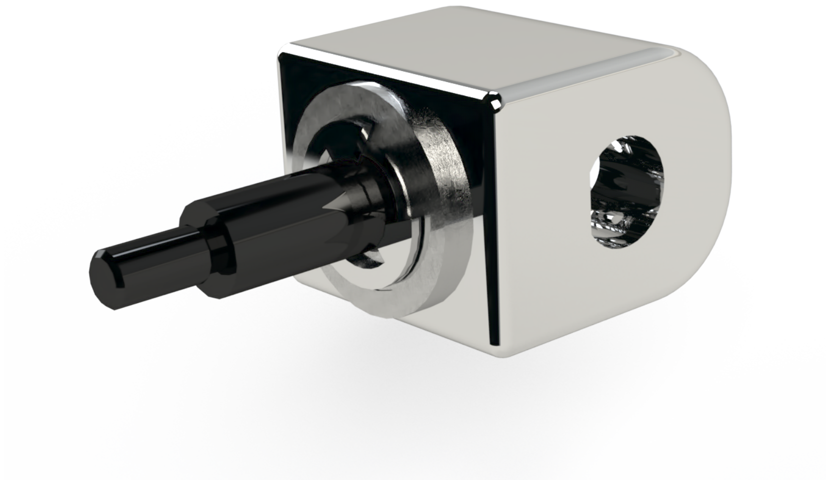

Figure 8-12: Connection joint between motor and arm with angular bearing assembly

Figure 8-13: Exploded view of motor joint with angular bearing assembly

(a) Flanged Bushing for ELBOW

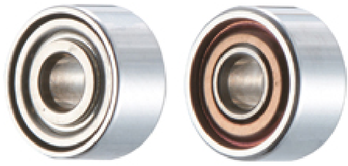

(b) Angular contact ball bearing

(c) Bearing Shaft Screws

(d) Self-lubricating Bushing for PLATFORM

(e) Washer

(f) Precision Pivot Pins

Figure 8-14: Mechanical Hardware used in the ABS Prototype [17]

Since in the other joints all the supported load needs to be completely radial a full bushings configuration was chosen. In Fig.8-15 and in Fig.8-16 are shown respectively the arms elbow and platform joint design.

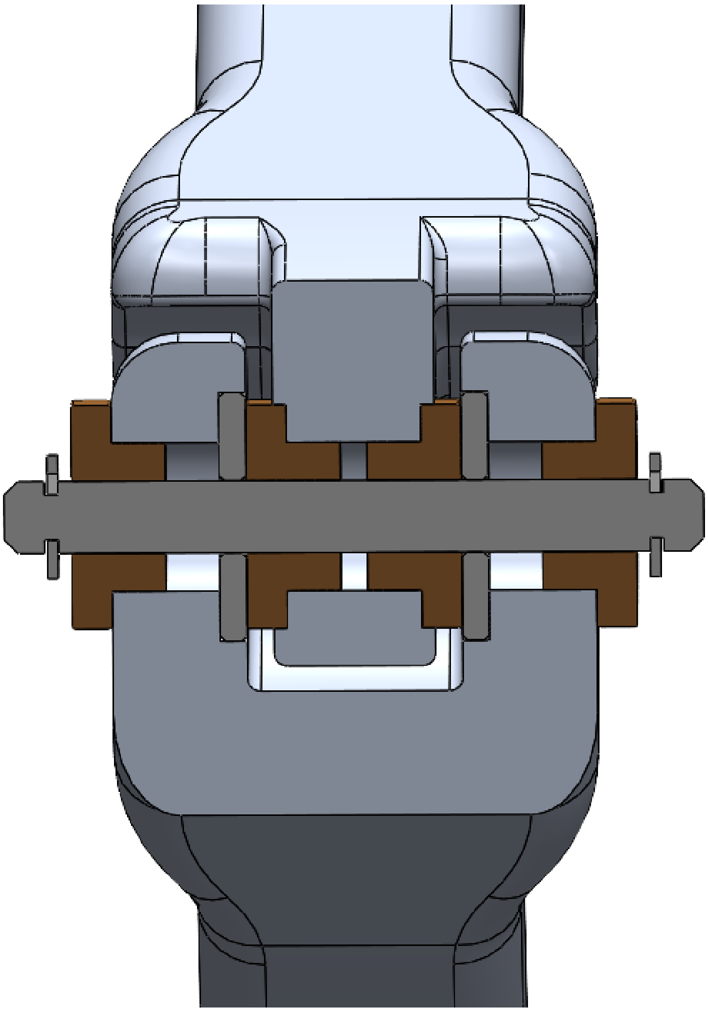

Figure 8-15: Section of elbow joint assembly

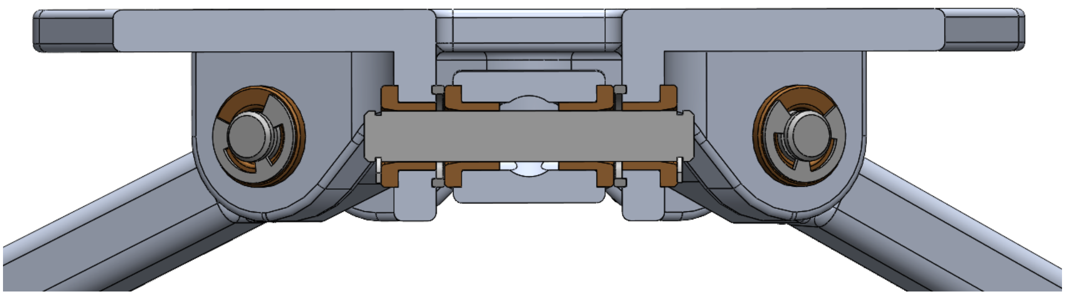

Figure 8-16: Section of joint assembly between the arm and the platform

As shown in both joint assemblies all the bushings selected are flanged since this allows the assembly to be axially constrained. An alignment shaft fixed with two side-mount external retaining rings.

The flanged bushing's surface goes in contact with a steel washer embedded in the lower arm in the case of Fig.8-15 and the platform structure in Fig.8-16.

The corresponding symmetric bushing is placed further apart from the other to allow the two joint assemblies to support great value or torsional load.

8-4 Base design

The main function of the base is to support the stepper motor rigidly and at the same time present mounting holes to allow to gimbal to be fixed to the satellite. To allow this function on the base are present vertical support with ribs and fixing holes on the base plate.
The base plate is designed in a way to protect the stepper motors and the encoders from possible impacts since the external perimeter of the plate surround the stepper motors and the encoders mounted on the same shaft of the motor as shown in Fig.8-17.

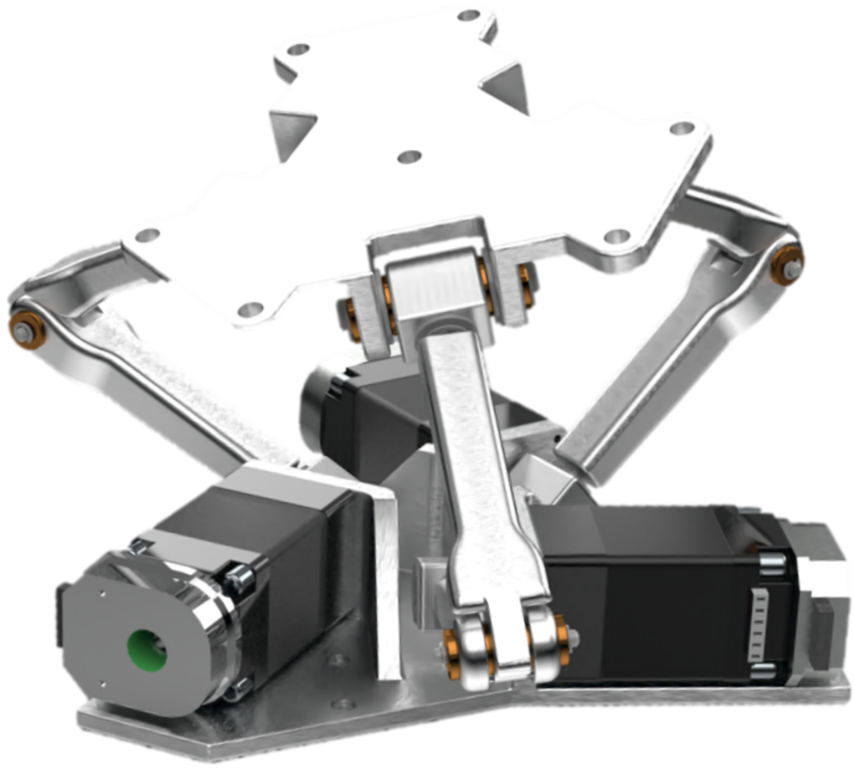

Figure 8-17: Base design view

Chapter 9

Strategic positioning and possible future development

As explained in section 3-3 the final developed gimbal will have some innovation keys compared to other pointing systems on the market.

The main differences in this system are:

- Arm design and dimensions optimized for the specific application with mechanical protection against failures
- Control and trajectory planning based on Reinforcement learning (RL) to allow the system to be more robust from a kinematic point of view, resilient for changes in the working environment, and adaptable to possible failures as explained by National Aeronautics and Space Administration (NASA) in the paper explained in section 3-2-5 [11].

This new RL based control system allows the manipulator to automatically generate also the best trajectory to reach the desired pointing goal in the workspace domain. To evaluate the Robot workspace dimensions in further development of this thesis it would be possible to represent a set of points reachable from the manipulator throw a capability map as described by the paper *"Capturing Robot Workspace Structure: Representing Robot Capabilities"* [18].

The versatility of this structure can also be used for other spacecraft applications. The gimbal can be used to provide high-power generation, large delta-V thrust, and precision pointing. In the paper, [19] Jonathan S. Wrobel investigates the application of the gimbal as the pointing system of the solar array to replace the Solar Array Drive Assemblies (SADA) to allow the pointing over a full hemisphere. Furthermore, the gimbal joint permits the thrust vector to be controlled relative to the center of mass of the CubeSat, which allows for both orbit adjustment and thrust-driven attitude control. During periods when the gimbal is not directing thrust events and solar collection, the joint allows the attitude of the payload section to be controlled by using the inertia of the CubeSat module. [19]. An image of the proposed configuration is shown in Fig.9-1 and Fig.9-2.

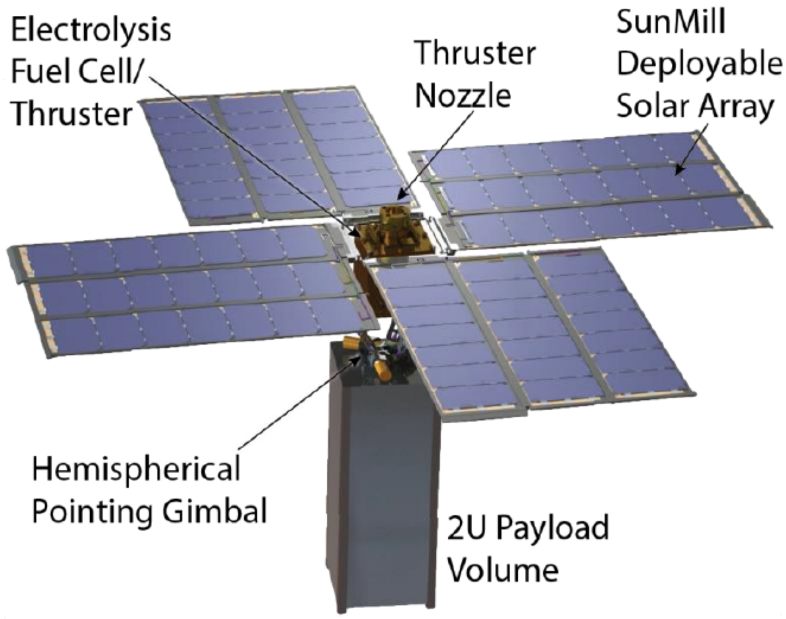

Figure 9-1: The PowerCube system with the major sub-systems called out [19]

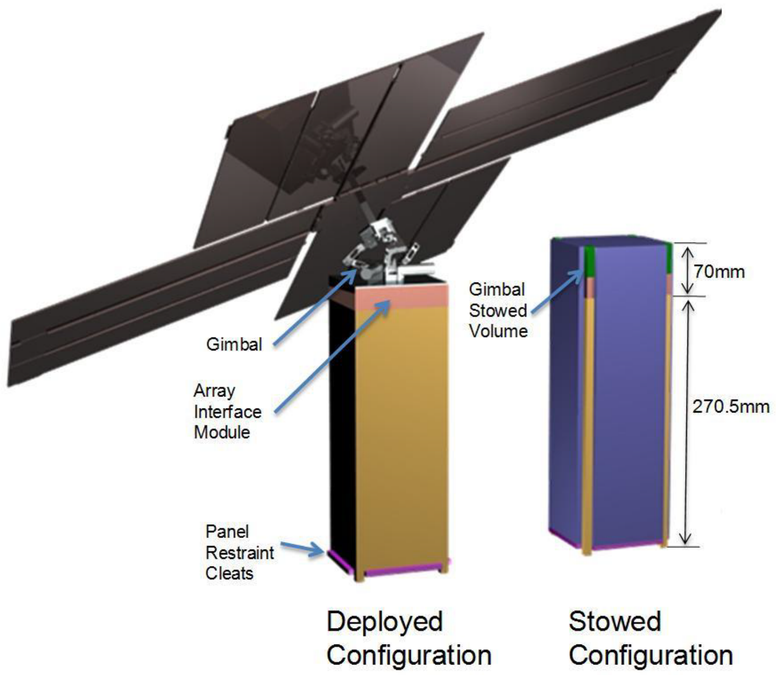

Figure 9-2: Deployed and stowed configurations of the array showing the stowed area in blue, with the rails (gold) exposed [19]

Chapter 10

Prototype Bill of Materials

From the previews analysis results, a Bill of materials (BOM) was produced with all the component necessary to produce a prototype.

The main objective of the prototype, as will be discussed in section 11 will be to:

- Controller testing and hardware in the loop tuning
- Predictive maintenance estimation
- Reinforcement learning control algorithm development and training
- Mechanical design tuning

To allow the development of these objectives, in this section the reason behind the selection of the various component will be explained.

10-1 Mechanical Hardware

For the mechanical hardware the focal points that guided the selection were:

- Cheap stock components
  to be able to lower the prototype price and to be easily replaced
- Material properties similar to the final flight hardware
  to be able to have adequate hardware in the loop simulation to analyze the components mechanical wear

The function of the various components presented in Fig.10-1 is discussed in section 8-3.

Item	Quantity		Price	TOT Price	Part number	Company
MECHANICAL HARDWARE						
Angular contact ball bearing	6		4,89 €	29,34 €	FL685ZZ	Misumi
Bearing Shaft Screws	6		23,47 €	140,82 €	BGSPSW5-8-L15-S5	Misumi
Precision Pivot Pins for ELBOW	3		1,47 €	4,41 €	CDG3-22	Misumi
Precision Pivot Pins for PLATFORM	3		2,20 €	6,60 €	CDG6-35	Misumi
ABS Resin for 3D printer	500	ml		70,00 €		
Flanged Bushing for ELBOW	12			73,56 €	54F-0303	Misumi
Self-lubricating Bushing for PLATFORM	12			28,05 €	MPFZU6-10	Misumi
Washer for ELBOW	6			6,72 €	WSSB10-4-1	Misumi
Washer for PLATFORM	6			9,18 €	WSSB15-8-1.5	Misumi
TOT MECHANICAL				**368,68 €**		

Figure 10-1: Mechanical prototype BOM list required to assemble the prototype

The first prototype is planned to be printed in ABS with a 3d printer since this technology is cheap and allows to check and easily modify the mechanical design before switching to a metal design. The prototype will then be produced in aluminum 7075 T6 with a Computer Numerical Control (CNC) machine to allow thermal and vibration testing of the system before proceeding in the construction of the Ground model (GM).

10-2 Electronic hardware

For the electronic hardware the focal points that guided the selection were:

- Cheap stock components
  to be able to lower the prototype price and to be easily replaced
- Good documentation and forum support
- Powerful enough to allow future control algorithm logic updates

In Fig.10-2 the BOM of the Electronic hardware is presented.

Item	Quantity		Price	TOT Price	Part number	Company
ELECTRONICS						
AC/DC Power Modules 150W 24V 6.3A	1		61,66 €	61,66 €	495-TXLN150-124	Mouser
Raspberry Pi 4 B, 4 GB	1		59 €	58,75 €	358-RPI4MODBP4GBBULK	Mouser
MOTORS						
NEMA11-20-02D-AMT112S	3		103 €	307,80 €	490-NEMA11202AMT112S	Mouser
SENSORS						
MPU-6050 Triple Axis Accelerometer and Gyro Breakout	1		25 €	25,37 €	474-SEN-11028	Mouser
STEPPER CONTROLLER						
RAMPS 1.4	1		15 €	14,64 €	RAMPS 1.4	C & D elettronica
Stepper driver A4988 con dissipatore	3		4 €	12,78 €	SDP1013	C & D elettronica
TOT ELECTRONICS				**481,00 €**		

Figure 10-2: Electronic hardware BOM

(a) Raspberry pi 4 Gb

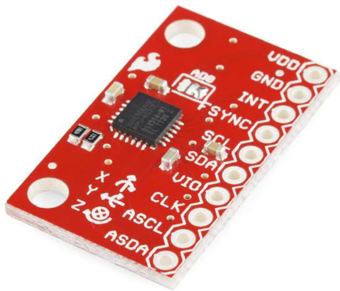

(b) MPU-6050 Triple Axis Accelerometer and Gyro

(c) NEMA11-20-02D-AMT112S

(d) AC/DC Power Modules 150W 24V 6.3A

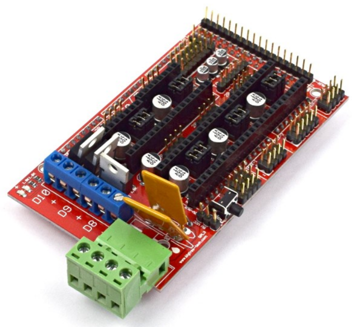

(e) RAMPS 1.4 Stepper controller

(f) Stepper driver A4988

Figure 10-3: Mechanical Hardware used in the ABS Prototype [17] and [20]

10-2-1 Central Processing Unit (CPU)

For the Processing Unit a Raspberry pi with 4 Gb of ram, shown in Fig.10-3a, was chosen since can run the Robot Operating System (ROS) [21] which is the standard operating system used in robotic applications. At the same time, this board is capable of handling a pre-trained Reinforcement learning (RL) algorithm when it will be developed to produce autonomously the trajectory planning and the control of the manipulator.

10-2-2 Motor

As discussed in section 7 the final motor that has been selected for the specific application is a stepper motor shown in Fig.10-3c. As shown from the final simulation 7-3, the torque required is $0.1Nm$. For this reason, a Nema 11 was selected since it has a max holding torque of $0,117Nm$ to guarantee some margin and mechanical dimensions suitable to the chosen design. The torque plot of the motor is shown in Fig. 10-4.

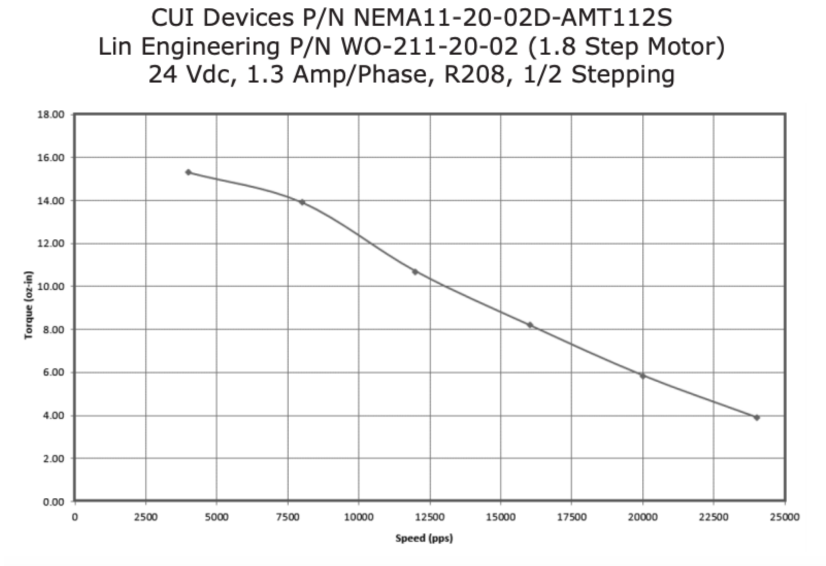

Figure 10-4: Nema 11 torque curve [22]

To be able to control if the actual command position sent to the motor is been reached and to compensate for possible position errors an encoder for closed-loop control was placed on the same motor axis. The motor and encoder assembly is shown in Fig.10-5

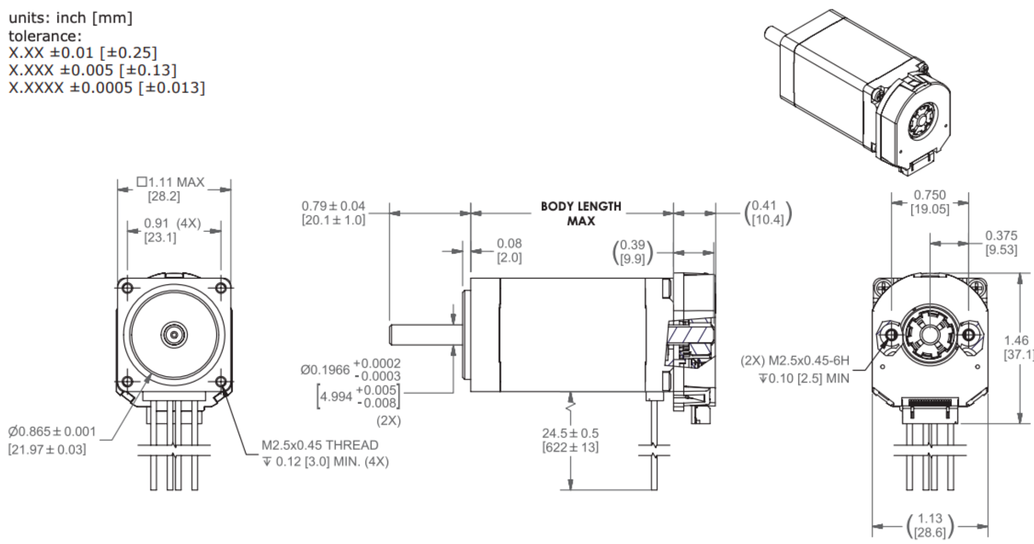

Figure 10-5: Nema 11 stepper motor with position encoder technical drawing [22]

10-2-3 Feedback sensors

For the sensor part of the manipulator, in addition to the optical encoders mounted directly to the motor shaft as shown in Fig.10-3c, a component called MPU-6050 has been selected since with its Triple Axis accelerometer and its Gyro is the perfect candidate to send data back to the CPU. The sensor will be mounted in the center of the platform and will return the orientation data that the end effector will experience. With this data, it will be possible to tune the controller and estimate the minimum pointing error that the pointing mechanism is able to achieve.

Chapter 11

Next steps

11-1 Prototype testing

- Mechanical testing correct motion of the structure
- Controller testing and hardware in the loop tuning
- Stepper position overshot measurement and compensating control development
- Central cable management testing and analysis
- Preliminary predictive maintenance estimation
- Reinforcement learning control and trajectory planning algorithm development and training
- Mechanical design tuning

In this first phase, the Inverse kinematics (IK) block outputs will be sent to a simple PID-based controller for testing purposes. In fact, the primary objective of the designed prototype is to test the correct mechanical motion and to test the control precision feasibility of the mechanism

11-2 Ground model (GM) Prototype

- Environmental
  - Thermal Cycles
  - Thermal Vacuum Chamber test (TVAC)
  - Vibe tests

- Deployment test with launch lock
- Position vibration testing
- Evaluation of angular momentum transferred to the satellite
- Mechanical design tuning with thermal data
- GM stepper motor testing
- Working life prediction analysis with predictive maintenance (Artificial intelligence (AI))

Glossary

List of Acronyms

AI	Artificial intelligence
BOM	Bill of materials
CoG	Centre of gravity
Dof	Degree of freedom
GM	Ground model
IK	Inverse kinematics
FK	Forward Kinematics
RL	Reinforcement learning
SADA	Solar Array Drive Assemblies
CNC	Computer Numerical Control
CPU	Central Processing Unit
ROS	Robot Operating System
TVAC	Thermal Vacuum Chamber test
NASA	National Aeronautics and Space Administration

Bibliography

[1] *ARGOTEC presents ANDROMEDA*, Argotec S.R.L., 2021. URL http://www.argotec.it/online/2020/04/21/argotec-presents-andromeda/, Last accessed: June 03, 2021.

[2] Vukobratović, M., *Introduction to Robotics*, Springer Berlin Heidelberg, 1989. doi:10.1007/978-3-642-82997-0.

[3] *Omni wrist family*, Ross-Hime Designs Inc., 2015. URL https://www.anthrobot.com/tech/, Last accessed: 2021-05-28.

[4] *Wide angle gimbal*, J. Sofka, 2021. URL http://sofka.org/portfolio/gimbal/, Last accessed: 01.09.2016.

[5] Merriam, E. G., Jones, J. E., Magleby, S. P., and Howell, L. L., "Monolithic 2 DOF fully compliant space pointing mechanism," *Mechanical Sciences*, Vol. 4, No. 2, 2013, pp. 381–390. DOI: 10.5194/ms-4-381-2013.

[6] Canfield, S. L., "Development of the carpal wrist; A symmetric, parallel-architecture robotic wrist," Ph.D. thesis, Virginia Tech, 1997.

[7] *Canfield Joint*, CEN and NASA Glenn Research facility, 2016. URL https://www.cem.utexas.edu/content/canfield-joint, Last accessed: 2021-06-04.

[8] Pagis, G., Bouton, N., Briot, S., and Martinet, P., "Enlarging Parallel Robot Workspace through Type-2 Singularity Crossing," *Control Engineering Practice*, Vol. 39, 2015, pp. 1–11. DOI: 10.1016/j.conengprac.2015.01.009.

[9] BILGIN, B., "VISUAL SERVOING FOR TARGET TRACKING USING A NON-LINEAR 2 DEGREE OF FREEDOM SYSTEM," Ph.D. thesis, MIDDLE EAST TECHNICAL UNIVERSITY, 2019.

[10] Nikulin, V., Khandekar, R., and Sofka, J., "Performance of a laser communication system with acousto-optic tracking: An experimental study," 2006. DOI: 10.1117/12.640112.

[11] Short, R., and Hylton, A., "A Topological Kinematic Workspace Analysis of the Canfield Joint," , 09 2018.

[12] *"Robotic Gimbals"*, Tethers Unlimited, 2021. URL https://www.tethers.com/robotic-gimbals/.

[13] "TRIPOD Gimbal For satellites," , 2021. URL https://comat-agora.com/products/tripod.

[14] Sebastian, C., "Robot Manipulation, Part 1: Kinematics," https://blogs.mathworks.com/racing-lounge/2018/04/11/robot-manipulation-part-1-kinematics/?s_eid=PSM_15028, 2018.

[15] Donges, N., "GRADIENT DESCENT: AN INTRODUCTION TO 1 OF MACHINE LEARNING'S MOST POPULAR ALGORITHMS," https://builtin.com/data-science/gradient-descent, 2019.

[16] Castro, S., "Robot Manipulation, Part 2: Dynamics and Control," , 2018. URL https://blogs.mathworks.com/racing-lounge/2018/04/25/robot-manipulation-part-2-dynamics-and-control/?s_eid=PSM_15028.

[17] *Mechanical hardware source*, Misumi Inc., 2021. URL https://it.misumi-ec.com/, Last accessed: 2021-05-21.

[18] Zacharias, F., Borst, C., and Hirzinger, G., "Capturing robot workspace structure: representing robot capabilities," *2007 IEEE/RSJ International Conference on Intelligent Robots and Systems*, IEEE, 2007. doi:10.1109/iros.2007.4399105.

[19] Wrobel, J., Hoyt, R., Slostad, J., Storrs, N., Cushings, J., Moser, T., Luise, J. S., and Jimmerson, G., "PowerCube(TM) - Enhanced Power, Propulsion, and Pointing to Enable Agile, High-Performance CubeSat Missions," *AIAA SPACE 2012 Conference & Exposition*, American Institute of Aeronautics and Astronautics, 2012. doi:10.2514/6.2012-5217.

[20] *Stepper controller source*, "C e D ELETTRONICA", 2021. URL https://www.cedelettronica.com/it/prodotti/automazione/scheda-controller-ramps-1-4/2588, Last accessed: 2021-06-05.

[21] *"Open Source Robot Operating System"*, ROS, 2021. URL https://www.ros.org/.

[22] *NEMA11 Stepper servo motor*, Mouser Inc., 2021. URL https://www.mouser.it/datasheet/2/670/nema11_amt112s-1778758.pdf, Last accessed: 2021-05-22.